

Morse theory study on the evolution of nodal lines in \mathcal{PT} -symmetric nodal-line semimetalsManabu Takeichi, Ryo Furuta, and Shuichi Murakami *Department of Physics, Tokyo Institute of Technology, 2-12-1 Ookayama, Meguro-ku, Tokyo 152-8551, Japan*

(Received 7 November 2022; revised 4 January 2023; accepted 17 January 2023; published 22 February 2023)

A nodal-line semimetal is a topological gapless phase containing one-dimensional degeneracies called nodal lines. The nodal lines are deformed by a continuous change of the system such as pressure and they can even change their topology, but it is not systematically understood what kind of changes of topology of nodal lines are possible. In this paper, we classify the events of topology change of nodal lines by the Morse theory and reveal that only three types of topology changes of nodal lines, i.e., creation, reconnection, and annihilation, are possible in the spinless nodal-line semimetal protected by inversion and time-reversal symmetries. They are characterized by an index having the values 0, 1, and 2 for the above three types in the Morse theory. Moreover, we extend our theory to systems with rotational symmetries and mirror symmetry and disclose the possible events of topology change of nodal lines under each symmetry.

DOI: [10.1103/PhysRevB.107.085139](https://doi.org/10.1103/PhysRevB.107.085139)**I. INTRODUCTION**

Topological phases of matter have been attracting much attention in condensed matter physics. The topological phases are classified into two cases: topological insulators [1–7] and topological semimetals [8–11]. The topological semimetals can hold either zero-dimensional (0D), one-dimensional (1D), or two-dimensional (2D) degeneracies in \mathbf{k} space between a conduction band and a valence band in three-dimensional (3D) materials. In the momentum space, a topological 0D degeneracy is Dirac points [12–14] and Weyl points [15–26], a topological 1D degeneracy is nodal lines [9,27], and a topological 2D degeneracy is nodal surfaces [28–34]. These gapless states are robust against perturbations because of symmetry or topological reasons. The topological semimetals possessing the nodal lines are called nodal-line semimetals, and the nodal lines have several varieties depending on the relative positions of nodal lines: nodal rings [35–41], nodal chains [42–44], nodal links [45–50], and so on. The nodal ring is a loop of the nodal line, the nodal chain has touching points of two nodal lines, and the nodal link forms a link between two nodal lines.

The nodal line is protected by crystal symmetry, such as mirror symmetry or a combination of inversion (\mathcal{P}) symmetry and time-reversal (\mathcal{T}) symmetry [9,10]. The nodal lines are confined on the mirror planes in the former case, and there are no constraints for the positions of nodal lines in the latter case. Meanwhile, the nodal lines are characterized by a quantized value of the Berry phase [51–53] in the latter. When the spin-orbit coupling (SOC) is negligible in systems considered, the Berry phase on any closed path is quantized to be 0 or π modulo 2π under \mathcal{PT} symmetry. The nodal line with \mathcal{PT} symmetry has a π Berry phase when the closed path links with the nodal line.

In this paper, we focus on the nodal lines protected by the π Berry phase. Under a continuous change of the system, the shapes of the nodal lines with the π Berry phase are deformed as long as the system keeps the \mathcal{PT} symmetry. In addition

to the deformations of the shapes of nodal lines, the nodal lines may change their connectivity, i.e., their topology. For example, through a continuous change of the system, two nodal lines may merge into one and vice versa.

In this paper, we show that the change of topology of nodal lines are classified in terms of the Morse theory and reveal that there are only three cases for the change of topology, i.e., creation, reconnection, and annihilation. We introduce the notion of the index in the Morse theory. Moreover, we classify the evolutions of nodal lines in systems with mirror or rotational symmetry. In these cases with additional crystallographic symmetry, the Morse theory cannot be directly applied and the index is not defined. Here, we find that in such cases the coefficient functions in the Hamiltonian is always “factorized,” and after the factorization one can apply the Morse theory to define the index and to classify the events of topology changes of nodal lines. Through this study, we exhaust all the possible events of topology changes of nodal lines. It also means that events of topology changes other than these listed in this paper do not occur. For example, a direct transition from two nodal lines to a nodal link cannot occur when no crystallographic symmetry is assumed.

This paper is organized as follows. In Sec. II, we show an example of the evolution of the nodal line in a previous study and the limitation of the model. In Sec. III, we reveal relationships between an index and a possible evolution of nodal line under \mathcal{PT} symmetry and classify the changes with indices. In Sec. IV, we show evolutions of nodal lines with an additional rotational or mirror symmetry. We summarize the paper in Sec. V.

II. NODAL LINES WITH π BERRY PHASE AND THEIR EVOLUTIONS**A. Nodal lines with the π Berry phase**

We study nodal lines in 3D spinless systems protected by the quantized π Berry phase. For this purpose, we need to

consider one conduction and one valence bands and a two-band Hamiltonian is written as

$$\mathcal{H}(\mathbf{k}) = a_0(\mathbf{k})\sigma_0 + \mathbf{a}(\mathbf{k}) \cdot \boldsymbol{\sigma}, \quad (1)$$

where $\mathbf{k} = (k_x, k_y, k_z)$, $a_0(\mathbf{k})$ and $\mathbf{a}(\mathbf{k}) = (a_x(\mathbf{k}), a_y(\mathbf{k}), a_z(\mathbf{k}))$ are real functions, σ_0 is the 2×2 identity matrix, and $\boldsymbol{\sigma} = (\sigma_x, \sigma_y, \sigma_z)$ are the Pauli matrices. We put $a_0(\mathbf{k}) = 0$ for simplicity because it does not affect the nodal lines. In the absence of SOC, \mathcal{PT} symmetry ensures that the Hamiltonian is real [$\mathcal{H}(\mathbf{k}) = \mathcal{H}^*(\mathbf{k})$], i.e., $a_y(\mathbf{k}) = 0$ under an appropriate gauge choice. The energy spectra are $E_{\pm}(\mathbf{k}) = \pm \sqrt{a_x^2(\mathbf{k}) + a_z^2(\mathbf{k})}$, and the positions of the nodal lines in \mathbf{k} space are obtained by solving $a_x(\mathbf{k}) = a_z(\mathbf{k}) = 0$. The Berry phase along a loop in the \mathbf{k} space in a system with \mathcal{PT} symmetry without SOC is quantized to 0 or π modulo 2π , and the nodal line is protected by the π Berry phase.

B. Change of topology of the nodal lines

In the previous study [46], a two-band model for a nodal link and a nodal chain is proposed, and the Hamiltonian $\mathcal{H}^{(A)}(\mathbf{k})$ is given as

$$\mathcal{H}^{(A)}(\mathbf{k}) = a_x^{(A)}(\mathbf{k})\sigma_x + a_z^{(A)}(\mathbf{k})\sigma_z, \quad (2)$$

$$a_x^{(A)}(\mathbf{k}) = 2 \sin k_x \sin k_z + 2f(\mathbf{k}) \sin k_y, \quad (3)$$

$$a_z^{(A)}(\mathbf{k}) = \sin^2 k_x + \sin^2 k_y - \sin^2 k_z - f^2(\mathbf{k}), \quad (4)$$

where $f(\mathbf{k}) = \sum_{i=x,y,z} \cos k_i - m$ and m is a real parameter. This two-band model exhibits two nodal rings for $m > 3$, a nodal chain with a touching point $\mathbf{k} = 0$ for $m = 3$, and a nodal link for $m < 3$. Namely, the nodal chain is an intermediate state between the nodal rings and the nodal link. However, we will show that this kind of a direct change between the nodal ring and the nodal link via the nodal chain does not occur in general, and this change in the model is permitted due to a special feature of the model, which is explained further below.

The nodal lines are regarded as intersections between two 2D closed surfaces $a_x^{(A)}(\mathbf{k}) = 0$ and $a_z^{(A)}(\mathbf{k}) = 0$ in the momentum space. By using this, we can calculate the tangential vector of the nodal line. The normal vector $\mathbf{n}^{(x)}$ of the closed surface $a_x^{(A)}(\mathbf{k}) = 0$ is parallel to $\nabla_{\mathbf{k}} a_x^{(A)} = (\frac{\partial a_x^{(A)}}{\partial k_x}, \frac{\partial a_x^{(A)}}{\partial k_y}, \frac{\partial a_x^{(A)}}{\partial k_z})$ with

$$\partial_{k_x} a_x^{(A)}(\mathbf{k}) = 2 \cos k_x \sin k_z - 2 \sin k_y \sin k_x, \quad (5)$$

$$\partial_{k_y} a_x^{(A)}(\mathbf{k}) = 2f(\mathbf{k}) \cos k_y - 2 \sin^2 k_y, \quad (6)$$

$$\partial_{k_z} a_x^{(A)}(\mathbf{k}) = 2 \cos k_x \sin k_z - 2 \sin k_y \sin k_z, \quad (7)$$

when $\nabla_{\mathbf{k}} a_x^{(A)} \neq 0$. Likewise, the normal vector $\mathbf{n}^{(z)}$ of the closed surface $a_z^{(A)}(\mathbf{k}) = 0$ is parallel to $\nabla_{\mathbf{k}} a_z^{(A)} = (\frac{\partial a_z^{(A)}}{\partial k_x}, \frac{\partial a_z^{(A)}}{\partial k_y}, \frac{\partial a_z^{(A)}}{\partial k_z})$ with

$$\partial_{k_x} a_z^{(A)}(\mathbf{k}) = 2 \sin k_x \cos k_x + 2f(\mathbf{k}) \sin k_x, \quad (8)$$

$$\partial_{k_y} a_z^{(A)}(\mathbf{k}) = 2 \sin k_y \cos k_y + 2f(\mathbf{k}) \sin k_y, \quad (9)$$

$$\partial_{k_z} a_z^{(A)}(\mathbf{k}) = -2 \sin k_z \cos k_z + 2f(\mathbf{k}) \sin k_z, \quad (10)$$

when $\nabla_{\mathbf{k}} a_z^{(A)} \neq 0$. Then, the tangential vector \mathbf{t} of the nodal line is determined as $\mathbf{t} \parallel (\mathbf{n}^{(x)} \times \mathbf{n}^{(z)})$.

Now we focus on the touching point of the nodal chain ($m = 3$), located at $\mathbf{k} = 0$. At the touching point ($\mathbf{k} = 0$) in the nodal chain ($m = 3$), we obtain $\nabla_{\mathbf{k}} a_x^{(A)}(0) = 0$ and $\nabla_{\mathbf{k}} a_z^{(A)}(0) = 0$, which means that the tangential vector is not determined. This is consistent with the shapes of the nodal lines, which cross perpendicularly at the touching point. Nonetheless, this result of vanishing values of $\nabla_{\mathbf{k}} a_x^{(A)} = (0, 0, 0)$ and $\nabla_{\mathbf{k}} a_z^{(A)} = (0, 0, 0)$ at the touching point does not come from physical reasons such as symmetry, but it is by accident. Since the Hamiltonian defined by Eqs. (3) and (4) has only the translation and \mathcal{PT} symmetries but no other crystallographic symmetry, this result of $\nabla_{\mathbf{k}} a_x^{(A)} = \nabla_{\mathbf{k}} a_z^{(A)} = 0$ cannot come from crystallographic symmetries. Hamiltonians for real materials are complicated, and there is no reason for these two vectors to be simultaneously zero at the touching point. Therefore the evolution of the nodal lines in this model may be unstable against perturbations.

Here we address a question whether such kinds of direct changes from nodal lines to nodal lines via nodal chains are possible. In a more general context, we study what kind of events are possible in general, which changes the topology of nodal lines. In the next section, we reveal what kind of events are allowed via the Morse theory.

III. EVOLUTIONS OF NODAL LINES WITHOUT ADDITIONAL SYMMETRIES

A. Example

In this section, we show three possible topology changes in the evolutions of nodal lines in the momentum space in two-band spinless Hamiltonians with \mathcal{PT} symmetry. The three possible changes of topology of nodal lines are reconnection, annihilation, and creation. In this section, we give Hamiltonians to show such changes, and in the next section, we present a general classification scheme for these events, to show that the topology changes are restricted to the above three types. The tangent vector of the nodal line, $\nabla_{\mathbf{k}} a_x \times \nabla_{\mathbf{k}} a_z$, is ill defined at the \mathbf{k} where the topology of nodal lines changes. This is natural because the nodal lines become points at the creation and annihilation or cross with other nodal lines at the reconnection.

1. Reconnection of nodal lines

When a Hamiltonian $\mathcal{H}^{(B)}(\mathbf{k})$ reads

$$\mathcal{H}^{(B)}(\mathbf{k}) = a_x^{(B)}(\mathbf{k})\sigma_x + a_z^{(B)}(\mathbf{k})\sigma_z, \quad (11)$$

$$a_x^{(B)}(\mathbf{k}) = \frac{1}{2}k_x^2 + k_y^2 + k_z^2 + \frac{1}{2}m^2 + k_x + 2m, \quad (12)$$

$$a_z^{(B)}(\mathbf{k}) = -\frac{1}{2}k_x^2 + \frac{1}{2}k_y^2 + \frac{3}{2}k_z^2 - \frac{1}{2}m^2 + k_x + m, \quad (13)$$

a reconnection of nodal lines happens at $m = 0$ as shown in Fig. 1(a). The red, black, and blue lines represent nodal lines with $m = -0.003$, 0, and 0.003, respectively. When m is changed from -0.003 to 0.003, two nodal lines approach each other, and they meet at $\mathbf{k} = 0$ when $m = 0$. Thereby they are reconnected and become two nodal lines which are different from those at $m < 0$.

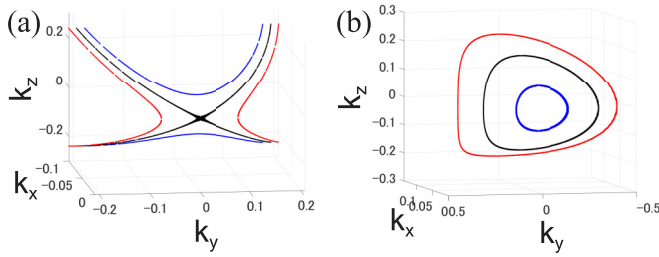


FIG. 1. Possible evolutions of nodal lines in the momentum space. (a) Reconnection of nodal lines in the Hamiltonian $\mathcal{H}^{(B)}(\mathbf{k})$. The red, black, and blue lines represent nodal lines with $m = -0.003$, 0 , and 0.003 , respectively. Two nodal lines touch at $m = 0$, and their reconnection happens as an intermediate state from nodal lines with $m = -0.003$ to different nodal lines with $m = 0.003$. (b) Annihilation (creation) of a nodal line by increasing (decreasing) the parameter m in the Hamiltonian $\mathcal{H}^{(C)}(\mathbf{k})$. The red, black, and blue lines represent nodal lines with $m = -0.1$, -0.05 , and -0.01 , respectively. The size of the nodal line gets smaller when m is increased, and there are no nodal lines in $m \geq 0$.

2. Annihilation of a nodal line

When a Hamiltonian $\mathcal{H}^{(C)}(\mathbf{k})$ is

$$\mathcal{H}^{(C)}(\mathbf{k}) = a_x^{(C)}(\mathbf{k})\sigma_x + a_z^{(C)}(\mathbf{k})\sigma_z, \quad (14)$$

$$a_x^{(C)}(\mathbf{k}) = \frac{1}{2}k_x^2 + k_y^2 + k_z^2 + \frac{1}{2}m^2 + k_x + 2m, \quad (15)$$

$$a_z^{(C)}(\mathbf{k}) = -\frac{1}{2}k_x^2 + \frac{1}{2}k_y^2 - \frac{1}{2}k_z^2 - \frac{1}{2}m^2 + k_x + m, \quad (16)$$

a nodal line is annihilated at $m = 0$ as shown in Fig. 1(b). The red, black, and blue lines represent nodal lines with $m = -0.1$, -0.05 , and -0.01 , respectively. When m is increased from -0.1 to -0.01 , the length of the nodal line gets shorter. The nodal line shrinks to a point at $\mathbf{k} = 0$ and is annihilated at $m = 0$. There is no nodal line when $m > 0$.

3. Creation of a nodal line

The process of creating a nodal line is a reverse process of annihilating a nodal line. Hence, the nodal line is created at $m = 0$ in Fig. 1(b) in decreasing the parameter m . Alternatively, the nodal line is created at $m = 0$ by increasing m after a transformation $m \rightarrow -m$ in Eqs. (14)–(16), and we label these transformed equations as $\mathcal{H}^{(D)}(\mathbf{k})$, $a_x^{(D)}(\mathbf{k})$ and $a_z^{(D)}(\mathbf{k})$. Within this transformed Hamiltonian, the red, black, and blue lines in Fig. 1(b) correspond to nodal lines with $m = 0.1$, 0.05 , and 0.01 , respectively.

We have shown three examples for a topology change in the evolutions of nodal lines in the momentum space above and we will introduce a notion of indices in the Morse theory in the next section, which will be used to classify these events.

B. Classification of topological changes of the nodal lines

The nodal lines evolve in the 3D \mathbf{k} space with changing m . For the purpose of classifying the events of their topology changes, we consider a four-dimensional (4D) (\mathbf{k}, m) space by adding a new axis of the parameter m into the 3D \mathbf{k} space, and the nodal lines in the 3D \mathbf{k} space are regarded as a 2D manifold M in the 4D (\mathbf{k}, m) space. In other words, conditions for nodal

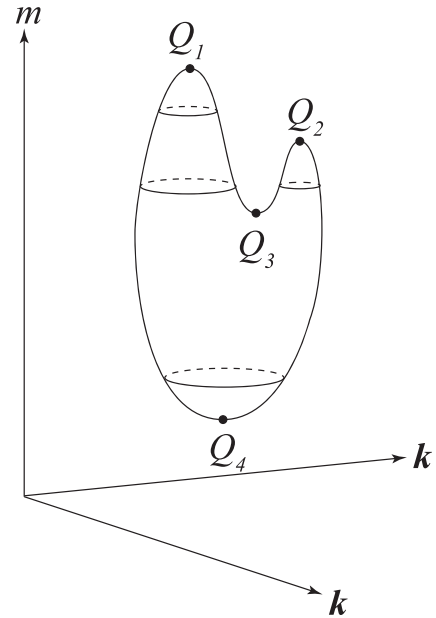


FIG. 2. An example of a 2D manifold in the 4D (\mathbf{k}, m) space, but the 3D \mathbf{k} space is described as a 2D \mathbf{k} space in the figure for the sake of illustration. There are four critical points of the function $f = m$: two local maxima at Q_1 and Q_2 , a saddle point at Q_3 , and a local minimum at Q_4 . As the contours of this manifold at fixed m give the nodal lines, the topology of the nodal lines changes when the value of m is changed across Q_i ($i = 1, 2, 3, 4$).

lines $a_x(\mathbf{k}) = 0$ and $a_z(\mathbf{k}) = 0$ compose the 2D manifold M in the 4D (\mathbf{k}, m) space because these two conditions lower the dimension by two. Let f denote a function $f : M \rightarrow \mathbb{R}$ giving the value of the parameter m for each point on M . Then, we show that the evolution of the nodal lines and their topology change are naturally described by the Morse theory [54,55]. In the Morse theory, we define a critical point Q on M as a point where the gradient of f is zero. In Fig. 2, we show a schematic figure of the critical point Q . The nodal lines change their topology by changing m across the critical point Q on the 2D manifold M . Each critical point Q is associated with an index, which is defined as the number of negative eigenvalues in the Hessian matrix of the function f on the 2D manifold M . Because the Hessian matrix contains all the second-order partial derivatives of the multivariable function, its eigenvalues discriminate a local maximum, a local minimum, and a saddle point of the function f . Therefore the index reveals the shape of the 2D manifold M around the critical point Q , and characterizes the topology change of the nodal lines. From the Morse theory we will show that the 2D manifold M is allowed to have three types of shapes around a critical point Q corresponding to the three types of topology change discussed in the previous section.

In our illustrative example of a 2D manifold M in Fig. 2, there are four critical points Q_i ($i = 1, 2, 3, 4$) for the function $f = m$. By noting that the nodal lines are the contours at $m = \text{const}$, one can see that the topology changes of the nodal lines occur at Q_i by changing the value of m . The function f has two local maxima at Q_1 and Q_2 , a saddle point at Q_3 , and a local minimum at Q_4 , and they correspond to the three types of

evolution of the nodal line, i.e., the annihilation, reconnection, and creation, respectively.

By following this scenario, we then rewrite the Hamiltonian defined in the 4D (\mathbf{k}, m) space $\mathcal{H}(\mathbf{k}) \rightarrow \mathcal{H}(\mathbf{k}, m)$, $a_j(\mathbf{k}) \rightarrow a_j(\mathbf{k}, m)$ ($j = x, z$), and $\nabla_{\mathbf{k}} \rightarrow \nabla_{\mathbf{k}, m} \equiv (\frac{\partial}{\partial \mathbf{k}}, \frac{\partial}{\partial m})$. Additionally, we introduce a function $f(\mathbf{k}, m) = m$ for calculation, where (\mathbf{k}, m) is a point on the 2D surface M .

Here, the 2D manifold M is defined by the two constraints $a_x = 0, a_z = 0$. Therefore, from the Kamiya theorem in the Morse theory [56] (see Appendix A), when a point Q is a critical point for the function f defined on the manifold M , $\nabla_{\mathbf{k}, m} f$ is a linear combination of $\nabla_{\mathbf{k}, m} a_x$ and $\nabla_{\mathbf{k}, m} a_z$. Namely, the following relation is satisfied:

$$\nabla_{\mathbf{k}, m} f(Q) = \alpha_x \nabla_{\mathbf{k}, m} a_x(Q) + \alpha_z \nabla_{\mathbf{k}, m} a_z(Q), \quad (17)$$

where α_x and α_z are real parameters. Furthermore, the index \mathcal{N} of the critical point Q is equal to the number of negative eigenvalues of the matrix

$$\mathcal{M} = \mathcal{P}(\mathcal{H}(f)|_Q - \alpha_x \mathcal{H}(a_x)|_Q - \alpha_z \mathcal{H}(a_z)|_Q) \mathcal{P}, \quad (18)$$

where the matrix \mathcal{P} represents an orthogonal projection to the 2D tangent vector space at the critical point Q , and \mathcal{H} is a Hessian matrix. For the further discussion, we need to restrict ourselves to the cases where the critical point is nondegenerate, which means that the matrix \mathcal{M} in Eq. (18) has no zero eigenvalue. Equation (18) is a 2×2 real symmetric matrix in terms of the basis of the tangent vector space, and so its index \mathcal{N} takes the values 0, 1, and 2. Using the Morse lemma (see Appendix B), we obtain the form of the function f around the critical point Q through the value of the index, and we will see that $\mathcal{N} = 2, 1, 0$ corresponds to annihilation, reconnection, and creation of nodal lines, respectively. To illustrate this feature, we consider the three Hamiltonians $\mathcal{H}^{(B)}$, $\mathcal{H}^{(C)}$, and $\mathcal{H}^{(D)}$ as examples to show how this theory works.

1. Reconnection of nodal lines

We consider the Hamiltonian $\mathcal{H}^{(B)}$ in Eq. (11) and examine the nature of the 2D surface M defined by $a_j^{(B)}(\mathbf{k}, m) = 0$ ($j = x, z$) around its critical point $(\mathbf{k}, m) = (0, 0)$ where the nodal lines are reconnected as shown in Fig. 1(a). The gradients of $a_j^{(B)}(\mathbf{k}, m)$ and f at $(\mathbf{k}, m) = (0, 0)$ are

$$\nabla_{\mathbf{k}, m} a_x^{(B)}(0, 0) = \begin{pmatrix} 1 \\ 0 \\ 0 \\ 2 \end{pmatrix}, \quad \nabla_{\mathbf{k}, m} a_z^{(B)}(0, 0) = \begin{pmatrix} 1 \\ 0 \\ 0 \\ 1 \end{pmatrix}, \quad (19)$$

$$\nabla_{\mathbf{k}, m} f(0, 0) = \begin{pmatrix} 0 \\ 0 \\ 0 \\ 1 \end{pmatrix}, \quad (20)$$

and we get the following relationship:

$$\nabla_{\mathbf{k}, m} f(0, 0) = \nabla_{\mathbf{k}, m} a_x^{(B)}(0, 0) - \nabla_{\mathbf{k}, m} a_z^{(B)}(0, 0). \quad (21)$$

This equation implies that $Q(0, 0)$ is a critical point by the Kamiya theorem explained in Appendix A, as expected. Basis vectors of the space spanned by the vectors in Eq. (19) are

given by

$$\mathbf{b}_1^{(B)} = \begin{pmatrix} 1 \\ 0 \\ 0 \\ 0 \end{pmatrix}, \quad \mathbf{b}_2^{(B)} = \begin{pmatrix} 0 \\ 0 \\ 0 \\ 1 \end{pmatrix}, \quad (22)$$

and an orthogonal projection to the tangent vector space at the critical point $Q(0, 0)$ is written as

$$\mathcal{P}^{(B)} = I_4 - \mathbf{b}_1^{(B)} \mathbf{b}_1^{(B)T} - \mathbf{b}_2^{(B)} \mathbf{b}_2^{(B)T} = \begin{pmatrix} 0 & & & \\ & 1 & & \\ & & 1 & \\ & & & 0 \end{pmatrix}. \quad (23)$$

Moreover, Hessian matrices of $a_j^{(B)}(\mathbf{k}, m)$ and $f(\mathbf{k}, m)$ at the critical point are obtained as

$$\mathcal{H}(a_x^{(B)})|_Q = \begin{pmatrix} 1 & & & \\ & 2 & & \\ & & 2 & \\ & & & 1 \end{pmatrix}, \quad (24)$$

$$\mathcal{H}(a_z^{(B)})|_Q = \begin{pmatrix} -1 & & & \\ & 1 & & \\ & & 3 & \\ & & & -1 \end{pmatrix}, \quad (25)$$

$$\mathcal{H}(f)|_Q = 0. \quad (26)$$

Therefore the matrix $\mathcal{M}^{(B)}$ is written as

$$\begin{aligned} \mathcal{M}^{(B)} &= \mathcal{P}^{(B)}(\mathcal{H}(f)|_Q - \mathcal{H}(a_x^{(B)})|_Q + \mathcal{H}(a_z^{(B)})|_Q) \mathcal{P}_B \\ &= \begin{pmatrix} 0 & & & \\ & -1 & & \\ & & 1 & \\ & & & 0 \end{pmatrix}, \end{aligned} \quad (27)$$

and it indicates that the critical point $Q(0, 0)$ is nondegenerate by the Kamiya theorem because the rank of $\mathcal{M}^{(B)}$ is 2, which is equal to the dimension of M . Furthermore, the index \mathcal{N} of f , defined as the number of the negative eigenvalues at the critical point $(0, 0)$ is 1.

Next we discuss the meaning of the index from the Morse lemma explained in Appendix B. Since $\mathcal{N} = 1$ we can set a local coordinate (k_1, k_2) along M around the critical point, which satisfies

$$k_1(Q) = k_2(Q) = 0, \quad (28)$$

$$f = f(Q) - k_1^2 + k_2^2. \quad (29)$$

This function f has a saddle point, as shown in Fig. 3(a), and reproduces the shape of the 2D manifold M around the critical point Q . The contour lines of this function f at $f = m$ are nodal lines. Thus, in Fig. 3(a) when we increase the value of m , the contour lines projected to the (k_1, k_2) plane, i.e., the nodal lines, are reconnected across the critical point Q . In that sense, a critical point Q with $\mathcal{N} = 1$ corresponds to the reconnection of nodal lines.

The nodal lines in this paper are characterized by the quantized π Berry phase, and this quantization is topologically

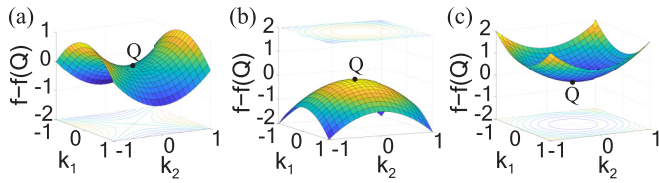


FIG. 3. Relationship between an index \mathcal{N} and a 2D surface M around a critical point Q . (a) The 3D graph of $f - f(Q) = -k_1^2 + k_2^2$ has a saddle point when $\mathcal{N} = 1$. The 2D surface M around the critical point Q locally has the same shape with this graph. Reconnection of nodal lines, which are contour lines in this figure, occurs at the critical point Q when we change contour lines from bottom to top by increasing $f(=m)$. (b) The 3D graph of $f - f(Q) = -k_1^2 - k_2^2$ has a local maximum when $\mathcal{N} = 2$. The 2D surface M around the critical point Q locally has the same shape with this graph. Annihilation of nodal lines, which are contour lines in this figure, occurs at the critical point Q when we change contour lines from bottom to top by increasing $f(=m)$. (c) The 3D graph of $f - f(Q) = k_1^2 + k_2^2$ has a local minimum when $\mathcal{N} = 0$. The 2D surface M around the critical point Q locally has the same shape with this graph. Creation of nodal lines, which are contour lines in this figure, occurs at the critical point Q when we change contour lines from bottom to top by increasing $f(=m)$.

protected in systems with \mathcal{PT} -symmetry without SOC. This π Berry phase is along a loop C encircling the nodal line [see Fig. 4(a)]. This quantized π Berry phase is very different from other topological invariants such as the Chern number or the Z_2 topological invariant, in that the Berry phase is associated with a specific loop C (and therefore it depends on the choice of the loop C), while the Chern number and the Z_2 topological invariant are associated with the entire occupied bands. Thus the π Berry phase along the loop C does not tell us about any information on the phases of the topological semimetal. Therefore the topology changes of the nodal lines such as reconnection, creation, and annihilation are not related with a change of any bulk topological invariant, and they do not correspond to topological phase transition.

Meanwhile, one can argue how the Berry phase is affected by the change of topology of nodal lines. As we explained, the Berry phase along the loop C encircling the nodal line [Fig. 4(a)] is equal to $\pi \pmod{2\pi}$. Along the loop C , the band gap is always open. Therefore, if the gap remains open on the loop C under the change of the system parameter m , the Berry phase remains constant. For example, in Fig. 4(b1) the Berry phase along the loop C_1 and C_2 are π and 2π , respectively. Then if the nodal lines in Fig. 4(b1) are reconnected, the nodal lines will look like Fig. 4(b2), where the Berry phase along the loop C_1 and C_2 are π and 0 , respectively. Thus, considering that the Berry phase is defined in terms of modulo 2π , the Berry phase is unaffected by the reconnection. It is also seen in Fig. 1. The Berry phase along a closed loop on the $k_z = 0$ plane encircling the two nodal lines (red lines) at $m = -0.003$ in Fig. 1(a). Via the change of m through $m = 0$ [the change from red to blue lines in Fig. 1(a)], the Berry phase changes from 2π to $0 \pmod{2\pi}$, which means that the Berry phase remains constant across the reconnection. It is natural because on the closed path, the system remains gapped and therefore the Berry phase cannot have a jump across the reconnection.

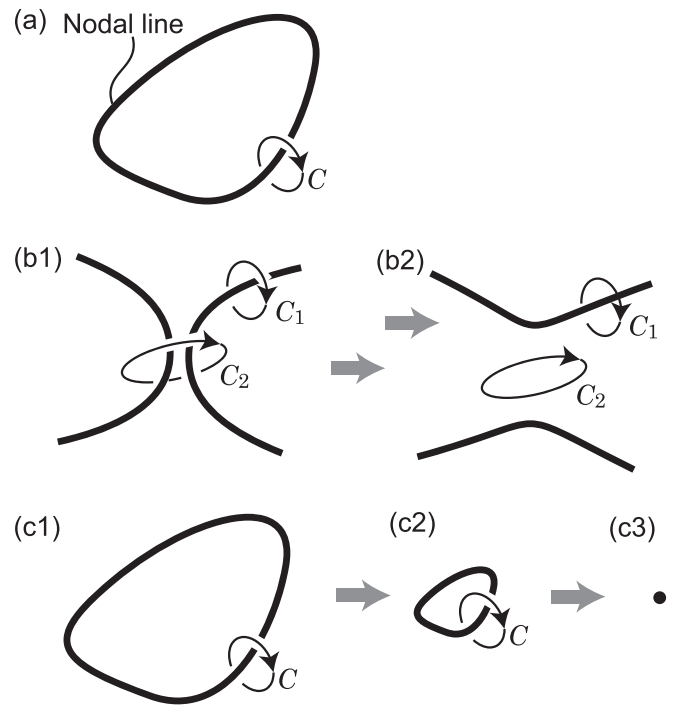


FIG. 4. Schematic figures for the quantized Berry phase around the nodal lines. (a) The Berry phase around the single nodal line is quantized to be π . (b) Across the reconnection, the Berry phases along C_1 and C_2 are preserved. (c) In the annihilation of the nodal line via the change of the parameter m , the Berry phase along the fixed loop C becomes undefined somewhere before the annihilation because the loop C crosses the nodal line.

On the other hand, suppose the nodal line in Fig. 4(c1) is annihilated as shown in Figs. 4(c2) and 4(c3). In this case, for the fixed loop C , it will eventually cross the nodal line *before* the nodal line shrinks to a point, and the Berry phase jumps from π to 0 . The value of m where this jump occurs depends on the position of the loop C , and it does not correspond to the value of m where the nodal line is annihilated. Thus the Berry phase for the specific loop C does not give any information on the topological phase.

2. Annihilation of a nodal line

We examine the nature of the 2D surface M defined by $a_j^{(C)}(\mathbf{k}, m) = 0$ ($j = x, z$) around its critical point $(\mathbf{k}, m) = (\hat{0}, 0)$ where the nodal line is annihilated as shown in Fig. 1(b). By the classification similar to Sec. III B1, the point $Q : (\mathbf{k}, m) = (0, 0)$ is a critical point of the function f with the index $\mathcal{N} = 2$.

From the Morse lemma, we can set a local coordinate (k_1, k_2) around the critical point, which satisfies

$$k_1(Q) = k_2(Q) = 0, \quad (30)$$

$$f = f(Q) - k_1^2 - k_2^2. \quad (31)$$

This function f means a local maximum of the 2D manifold M around the critical point Q , as shown in Fig. 3(b). When we increase the value of m , the contour line projected to the

(k_1, k_2) plane vanishes. Hence, a critical point Q with $\mathcal{N} = 2$ leads to the annihilation of nodal lines.

3. Creation of a nodal line

We examine the nature of the 2D surface M defined by $a_j^{(D)}(\mathbf{k}, m) = 0$ ($j = x, z$) around the critical point $(\mathbf{k}, m) = (0, 0)$, having the index $\mathcal{N} = 0$, where the nodal line is created as shown in Fig. 1(c).

From the Morse lemma, we can set a local coordinate (k_1, k_2) around the critical point, which satisfies

$$k_1(Q) = k_2(Q) = 0, \quad (32)$$

$$f = f(Q) + k_1^2 + k_2^2. \quad (33)$$

This function f has a local minimum around the critical point Q , as shown in Fig. 3(c). The change of the contour line projected to the (k_1, k_2) plane obtained by increasing the value of m reveals the creation of the nodal line. Thus a critical point Q with $\mathcal{N} = 0$ indicates the creation of nodal lines.

C. Results of a speciality removed model for the nodal link

As we discussed in Sec. II B, in the model described by Eqs. (2)–(4), both $\nabla_k a_x^{(A)}$ and $\nabla_k a_z^{(A)}$ vanish at the touching point of the nodal chain. This does not come from physical reasons such as symmetry, and is considered as an artifact of the special choice of the model. We can remove this artifact by adding some terms to the Hamiltonian. For example, we redefine the Hamiltonian by $a_x^{(A)} \rightarrow a_x'^{(A)} = a_x^{(A)} + \alpha \sin k_x$ and $a_z^{(A)} \rightarrow a_z'^{(A)} = a_z^{(A)} + \alpha \sin k_z$, where α is a real parameter. Then, as shown in Appendix D, instead of the direct transition from the nodal lines to a nodal chain, a reconnection of nodal lines occur three times to get a nodal chain.

In fact, this is expected from the Morse theory in this section. If we assume no crystallographic symmetry except for translation and \mathcal{PT} symmetries, the discussion in this section tells us that the topology change of nodal lines are restricted to three types, creation, reconnection, and annihilation. Meanwhile, the model (2)–(4) in Sec. II exhibits a direct transition from nodal lines to a nodal link, and this event is not among the three types described above. This means that the model (2)–(4) is not general but specially designed, and this transition from nodal lines to a nodal link is unstable against perturbations. Namely, from nodal lines to a nodal link, one cannot have direct transition, but it can be realized through multiple reconnections of nodal lines, if no additional crystallographic symmetries are assumed.

D. Short summary of this section

In this section, we reveal that there are three possible events of topology change of nodal lines from the above calculations. These events are characterized by the index \mathcal{N} from the Morse theory, and $\mathcal{N} = 2, 1$, and 0 corresponds to the annihilation, the reconnection, and the creation of nodal lines, as schematically shown in Figs. 5(a), 5(b) and 5(c), respectively, where $f(=m)$ is a parameter driving the evolution of nodal lines. The topology change of the nodal line in the vicinity of the critical point is illustrated in terms of the 2D local coordinates around the critical point in Fig. 3.

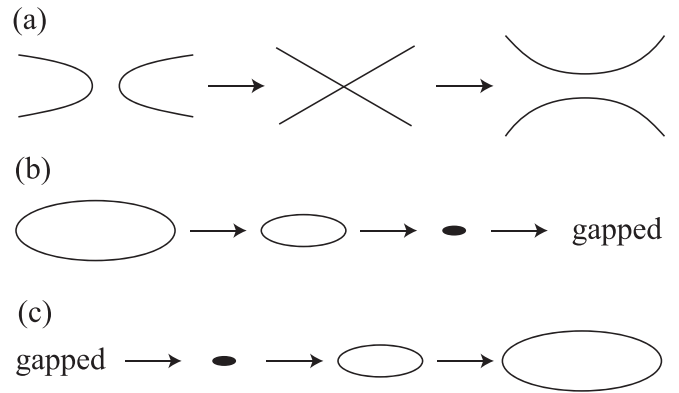


FIG. 5. Evolution of nodal lines with \mathcal{PT} symmetry in the momentum space. (a) The reconnection of nodal lines happen in the middle panel. (b) The nodal line is annihilated from the left panel to the right panel. (c) The nodal line is created from the left panel to the right panel.

IV. EVOLUTIONS OF NODAL LINES IN SYSTEMS WITH ADDITIONAL SYMMETRIES

This section shows topology changes of nodal lines with additional crystallographic symmetries in \mathcal{PT} -symmetric systems. For this purpose, we characterize the topology change in terms of the index \mathcal{N} in the Morse theory, by using $\mathbf{k} \cdot \mathbf{p}$ models with rotational or mirror symmetry.

We start with the 2×2 Hamiltonian $\mathcal{H}(\mathbf{k}) = a_x(\mathbf{k})\sigma_x + a_z(\mathbf{k})\sigma_z$ with \mathcal{PT} symmetry. In the presence of other crystallographic symmetries, we focus on a topology change of nodal lines at the \mathbf{k} point invariant under this crystallographic symmetry, and let \mathcal{G} denote the little group at this \mathbf{k} point. Then, the 2×2 effective Hamiltonian around that point satisfies

$$D(g)\mathcal{H}(\mathbf{k})D^{-1}(g) = \mathcal{H}(g\mathbf{k}) \quad \forall g \in \mathcal{G}, \quad (34)$$

where $D(g)$ is a representation matrix of the symmetry operation $g \in \mathcal{G}$. In the following, we consider the cases with C_n symmetry and with mirror symmetry.

A. Cases with C_n symmetries ($n = 2, 3, 4$, and 6)

Among various rotational symmetries, only the n -fold rotational (C_n) symmetry with $n = 2, 3, 4$, and 6 is allowed in crystals. We show how a nodal line evolves under the rotational symmetries.

1. C_2 symmetry

We consider nodal lines with \mathcal{PT} symmetry and twofold rotational symmetry with respect to the k_z axis. In spinless systems, the eigenvalue of C_2 is 1 for the irreducible representation (irrep) A and -1 for the irrep B, and we use conventional names for irreps known as Mulliken symbols [57,58]. We discuss topology changes of nodal lines at a point $\mathbf{k} = \mathbf{k}_0$ on the C_2 axis (k_z axis). Let us consider the case where one of the two bands follows the irrep A and the other follows the irrep B. Later in Sec. IV B, we consider the case with the two bands following the same irreps. Then, a representation

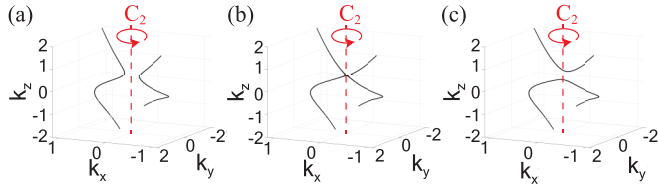


FIG. 6. Evolutions of nodal lines with the C_2 symmetry in the momentum space. Nodal lines are given by the Hamiltonian $\mathcal{H}^{(C_2)}(\mathbf{k})$ with $c_1 = 1$, $c_2 = \frac{1}{2}$, $c_3 = \frac{1}{4}$, $c_4 = \frac{1}{2}$, $c_5 = 1$, $c_6 = 1$, $c_7 = -1$, $c_8 = 1$, and $c_9 = 1$. (a), (b), and (c) represent nodal lines with $m = -0.3$, -0.25 , and -0.2 , respectively. The nodal lines are reconnected at $m = -0.25$ in (b).

matrix of the C_2 rotation is obtained as

$$D(C_2) = \begin{pmatrix} 1 & 0 \\ 0 & -1 \end{pmatrix}. \quad (35)$$

We shift the origin in \mathbf{k} space by \mathbf{k}_0 , so that the focused point becomes $\mathbf{k} = 0$. By using Eq. (34), the $\mathbf{k} \cdot \mathbf{p}$ Hamiltonian around $\mathbf{k} = 0$ is written up to the second order in \mathbf{k} as

$$\mathcal{H}^{(C_2)}(\mathbf{k}) = a_x^{(C_2)}\sigma_x + a_z^{(C_2)}\sigma_z, \quad (36)$$

$$a_x^{(C_2)}(\mathbf{k}) = c_1k_xk_z + c_2k_yk_z + c_3k_x + c_4k_y, \quad (37)$$

$$a_z^{(C_2)}(\mathbf{k}) = c_5k_x^2 + c_6k_y^2 + c_7k_z^2 + c_8k_xk_y + c_9k_z + m, \quad (38)$$

where c_i ($i = 1, 2, \dots, 9$) and m are real parameters. We set $c_1 = 1$, $c_2 = \frac{1}{2}$, $c_3 = \frac{1}{4}$, $c_4 = \frac{1}{2}$, $c_5 = 1$, $c_6 = 1$, $c_7 = -1$, $c_8 = 1$, and $c_9 = 1$ as an example. The parameter m , which plays a role of driving the evolution of nodal lines, is introduced as a constant term in Eq. (38) for simplicity. As shown in Fig. 6, a reconnection of nodal lines happens. Figures 6(a), 6(b) and 6(c) represent nodal lines with $m = -0.3$, -0.25 , -0.2 , respectively. When m is changed from $m = -0.3$ to -0.2 , the nodal lines are reconnected at $\mathbf{k} = (0, 0, \frac{1}{2})$ with $m = -\frac{1}{4}$. By the calculation similar to Sec. III B, we find that the point $(\mathbf{k}, m) = (0, 0, \frac{1}{2}, -\frac{1}{4})$ is a critical point with index $\mathcal{N} = 1$ by the Kamiya theorem. Then the reconnection of the nodal lines must occur by the Morse lemma, in agreement with Fig. 6.

Next, we generalize the result on the model Hamiltonian (36), and consider $a_x(\mathbf{k})$ and $a_z(\mathbf{k})$ as general analytic functions of \mathbf{k} . Because of Eq. (34), they follow $a_x(k_x, k_y, k_z) = -a_x(-k_x, -k_y, k_z)$ and $a_z(k_x, k_y, k_z) = a_z(-k_x, -k_y, k_z)$. Then, the gradients of the functions f , a_x , and a_z for the Morse theory at a point on the C_2 axis (k_z axis) are obtained as

$$\nabla_{\mathbf{k},m}f(0, 0, k_z, m) = (0, 0, 0, 1)^T, \quad (39)$$

$$\nabla_{\mathbf{k},m}a_x(0, 0, k_z, m) = (\cdot, \cdot, 0, 0)^T, \quad (40)$$

$$\nabla_{\mathbf{k},m}a_z(0, 0, k_z, m) = (0, 0, \cdot, \cdot)^T, \quad (41)$$

where \cdot represents a term left undetermined only from the symmetry, and such a term is in general nonzero. If there is a point $(0, 0, k_z, m)$ where Eqs. (39)–(41) are linearly dependent, the point is a critical point by the Kamiya theorem. It occurs when $\frac{\partial a_z}{\partial k_z} = 0$, leading $\nabla_{\mathbf{k},m}f \propto \nabla_{\mathbf{k},m}a_z$. Therefore

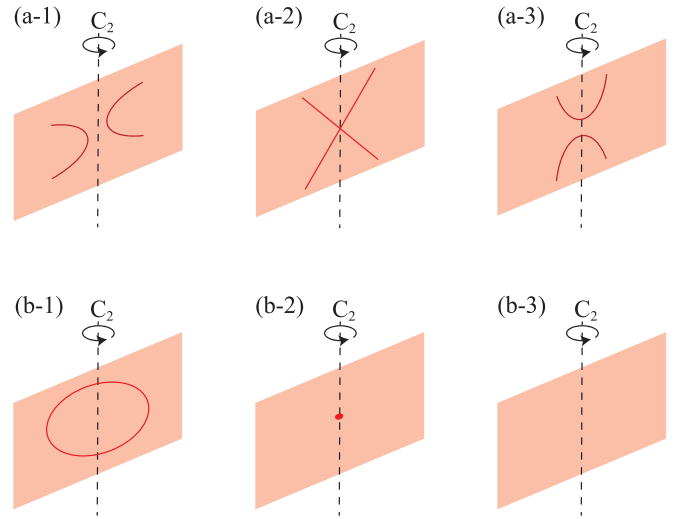


FIG. 7. Schematic pictures for the topology changes of nodal lines with the twofold rotational symmetry in the momentum space. The red colored nodal lines reside inside the C_2 -symmetric red plane near the C_2 axis. The reconnection of nodal lines occurs in (a-1)–(a-3), and the annihilation or creation occur in (b-1)–(b-3). We note that away from the C_2 axis, the nodal lines can be away from the red plane.

the critical point $(\mathbf{k}, m) = (0, 0, k_z, m)$ is determined by two conditions, $a_z = 0$ and $\frac{\partial a_z}{\partial k_z} = 0$, because on the C_2 axis, $a_x(0, 0, k_z, m)$ vanishes because of symmetry. Since the number of equations is equal to the number of variables (k_z, m), they can have solutions which are isolated points in the (\mathbf{k}, m) space in general. Then, the eigenvalues of the 2×2 matrix \mathcal{M} are nonzero in general, and the critical point is classified in terms of the index \mathcal{N} into three cases, $\mathcal{N} = 0, 1$, and 2 , corresponding to creation, reconnection, and annihilation of nodal lines, respectively.

In order to see how the nodal lines evolve under C_2 symmetry, we note that the vector $\nabla_{\mathbf{k}}a_x|_P = (\cdot, \cdot, 0)$ at the critical point P on the C_2 axis defines a normal vector of the surface $a_x = 0$. Thus, in the vicinity of the critical point P , the nodal lines evolve along the plane normal to this vector $\nabla_{\mathbf{k}}a_x|_P = (\cdot, \cdot, 0)$. This plane is C_2 -symmetric and it contains the C_2 axis as shown in Fig. 7. The red lines represent nodal lines, which lie along the red plane containing C_2 axis, and the nodal lines follow C_2 symmetry. For example, when $\mathcal{N} = 1$ and the reconnection happens, the nodal lines evolve from Figs. 7(a-1) to 7(a-3) through 7(a-2), and vice versa. This result from symmetry and the Morse theory matches with that of the numerical calculation in Fig. 6 in the vicinity of the critical point. Next when $\mathcal{N} = 2$ and the annihilation happens, the nodal lines evolve from Figs. 7(b-1) to 7(b-3) through 7(b-2). The nodal ring shrinks to a point on C_2 axis as shown in Fig. 7(b-2). Then, the case with $\mathcal{N} = 0$ corresponds to the creation of nodal lines, and is a reverse process, from Figs. 7(b-3) to 7(b-1).

2. C_3 symmetry

We consider nodal lines with \mathcal{PT} symmetry and threefold rotational symmetry with respect to the k_z axis. In spinless

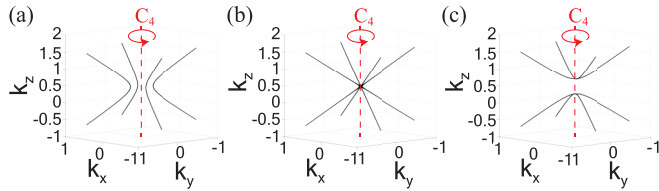


FIG. 8. Evolutions of nodal lines with the fourfold rotational symmetry in the momentum space. Nodal lines are given by the Hamiltonian $\mathcal{H}^{(C_4)}(\mathbf{k})$ with $c_1 = 1$, $c_2 = 2$, $c_3 = 1$, $c_4 = -1$, and $c_5 = 1$. (a), (b), and (c) represent nodal lines with $m = -0.3$, -0.25 , and -0.2 , respectively. The nodal lines are reconnected at $m = -0.25$ in (b).

systems, the eigenvalue of C_3 is 1 for the irrep A, $e^{2\pi i/3}$ for the irrep 2E , and $e^{-2\pi i/3}$ for the irrep 1E . Under the \mathcal{PT} symmetry, the irreps 1E and 2E are degenerate because they are complex representations, and a nodal line formed by 1E and 2E irreps always lies along the C_3 axis. Therefore it is impossible to see the topology change reflecting C_3 symmetry, and we can exclude this case from our discussion.

3. C_4 symmetry

We consider nodal lines with \mathcal{PT} symmetry and fourfold rotational symmetry with respect to the k_z axis. We discuss topology changes of nodal lines at a point $\mathbf{k} = \mathbf{k}_0$ on the C_4 axis (k_z axis). In spinless systems, the eigenvalue of C_4 is 1 for the irrep A, -1 for the irrep B, i for the irrep 2E , and $-i$ for the irrep 1E . We can exclude the irreps 1E and 2E from our discussion because under the \mathcal{PT} symmetry the complex irreps 1E and 2E are degenerate. Therefore let us consider the case where one of the two bands follows the irrep A and the other follows the irrep B. The cases with the two bands following the same irrep A (or B) will be discussed in Sec. IV B. Then, the representation matrix for C_4 is obtained as

$$D(C_4) = \begin{pmatrix} 1 & 0 \\ 0 & -1 \end{pmatrix}. \quad (42)$$

We focus on a point \mathbf{k}_0 on the C_4 axis. For convenience, we shift the origin in \mathbf{k} space by \mathbf{k}_0 , so that the focused point becomes $\mathbf{k} = 0$.

Now we discuss the evolution of nodal lines under the C_4 symmetry with Eq. (42). We begin with a simple example; by using Eq. (34), the $\mathbf{k} \cdot \mathbf{p}$ Hamiltonian around $\mathbf{k} = 0$ is written up to the second order in \mathbf{k} as

$$\mathcal{H}^{(C_4)}(\mathbf{k}) = a_x^{(C_4)}\sigma_x + a_z^{(C_4)}\sigma_z, \quad (43)$$

$$a_x^{(C_4)}(\mathbf{k}) = c_1(k_x^2 - k_y^2) + c_2k_xk_y, \quad (44)$$

$$a_z^{(C_4)}(\mathbf{k}) = c_3(k_x^2 + k_y^2) + c_4k_z^2 + c_5k_z + m, \quad (45)$$

where c_i ($i = 1, 2, \dots, 5$) and m are real parameters. We set $c_1 = 1$, $c_2 = 2$, $c_3 = 1$, $c_4 = -1$, and $c_5 = 1$ as an example. We show the result in Fig. 8, where nodal lines are reconnected by increasing m . Figures 8(a), 8(b) and 8(c) represent nodal lines with $m = -0.3$, -0.25 , and -0.2 , respectively. When m is changed from $m = -0.3$ to $m = -0.2$, the nodal lines are reconnected at $\mathbf{k} = (0, 0, \frac{1}{2})$ with

$m = -\frac{1}{4}$. Next, we want to characterize the point $P(\mathbf{k}, m) = (0, 0, \frac{1}{2}, -\frac{1}{4})$ by the Morse theory. Nevertheless, within our scenario in the previous sections, this point is not a critical point in the Morse theory since $\nabla_{\mathbf{k}} a_x^{(C_4)} = 0$ at this point. As a result, one cannot study this reconnection in terms of the Morse theory.

Here we find that by adopting the following argument of factorization this point P can be regarded as a nondegenerate critical point in the Morse theory, and then the classification in terms of the index \mathcal{N} can now be used. First, we note that $a_x^{(C_4)}$ can be factorized under the C_4 symmetry:

$$\begin{aligned} a_x^{(C_4)}(\mathbf{k}) &= ((\sqrt{2} - 1)k_x + k_y)((\sqrt{2} + 1)k_x - k_y) \\ &\equiv a_x^{(C_4)(I)}(\mathbf{k})a_x^{(C_4)(II)}(\mathbf{k}), \end{aligned} \quad (46)$$

where $a_x^{(C_4)(I)}(\mathbf{k}) = (\sqrt{2} - 1)k_x + k_y$, and $a_x^{(C_4)(II)}(\mathbf{k}) = (\sqrt{2} + 1)k_x - k_y$. Equation (46) means that $a_x^{(C_4)}(\mathbf{k})$ changes its sign four times around the k_z axis as is expected from the symmetry constraint $a_x^{(C_4)}(\mathbf{k}) = -a_x^{(C_4)}(C_4\mathbf{k})$. Therefore the condition for nodal lines is decomposed as

$$\begin{aligned} \text{(I)} \quad &a_x^{(C_4)(I)}(\mathbf{k}) = 0 \text{ and } a_z^{(C_4)}(\mathbf{k}) = 0, \\ \text{(II)} \quad &a_x^{(C_4)(II)}(\mathbf{k}) = 0 \text{ and } a_z^{(C_4)}(\mathbf{k}) = 0. \end{aligned}$$

We discuss a change of topology of nodal lines in cases (I) and (II) separately. In both cases (I) and (II), the point $(\mathbf{k}, m) = (0, 0, \frac{1}{2}, -\frac{1}{4})$ now becomes a critical point with index $\mathcal{N} = 1$ by the Kamiya theorem. At this critical point, the reconnections of nodal lines occur on $a_x^{(C_4)(I)}(\mathbf{k}) = (\sqrt{2} - 1)k_x + k_y = 0$ and $a_x^{(C_4)(II)}(\mathbf{k}) = (\sqrt{2} + 1)k_x - k_y = 0$ planes by the Morse lemma. The change of topology of nodal lines occurs in a C_4 -symmetric way because cases (I) and (II) are related to each other by C_4 symmetry.

Even apart from the example in Eqs. (43)–(45), in general C_4 -symmetric systems we can show that the topology change of nodal lines is fully characterized by the index \mathcal{N} for critical points. As seen in the above example, the key finding is that $a_x(\mathbf{k})$ can always be factorized under the C_4 symmetry. Then, by using each factor of a_x (not a_x itself), the points of the topology change of nodal lines become nondegenerate critical points in the Morse theory. To see this we assume that $a_x(\mathbf{k})$ and $a_z(\mathbf{k})$ are analytic in \mathbf{k} around the critical point $(0, 0, k_z^{(0)})$ and can generally contain higher order terms in \mathbf{k} . Even then, we show that $a_x(\mathbf{k})$ is factorized:

$$\begin{aligned} a_x(\mathbf{k}) &= i(\alpha k_+ g(\mathbf{k}) - \bar{\alpha} k_- \bar{g}(\mathbf{k}))(\alpha k_+ g(\mathbf{k}) + \bar{\alpha} k_- \bar{g}(\mathbf{k})), \\ &\equiv i a_x^{(-)}(\mathbf{k}) a_x^{(+)}(\mathbf{k}), \end{aligned} \quad (47)$$

where $a_x^{(\pm)}(\mathbf{k}) = \alpha k_+ g(\mathbf{k}) \pm \bar{\alpha} k_- \bar{g}(\mathbf{k})$, $k_{\pm} = k_x \pm ik_y$, and α is a complex constant. The function $g(\mathbf{k})$ is analytic in \mathbf{k} and satisfies $g(0, 0, k_z^{(0)}) = 1$ and $g(\mathbf{k}) = g(C_4\mathbf{k})$. The detailed proof of Eq. (47) is in Appendix E 1. Hence, nodal lines appear in the following cases:

$$\begin{aligned} \text{(I)} \quad &a_x^{(-)}(\mathbf{k}) = 0 \text{ and } a_z(\mathbf{k}) = 0, \\ \text{(II)} \quad &a_x^{(+)}(\mathbf{k}) = 0 \text{ and } a_z(\mathbf{k}) = 0. \end{aligned}$$

Because $a_x^{(\pm)}(C_4\mathbf{k}) = i a_x^{(\mp)}(\mathbf{k})$, $a_x^{(\pm)}(C_2\mathbf{k}) = -a_x^{(\pm)}(\mathbf{k})$, and $a_x^{(\pm)}(0, 0, k_z^{(0)}) = 0$, each of the equations $a_x^{(\pm)}(\mathbf{k}) = 0$ represents a C_2 -symmetric surface containing the rotational axis, and the combination of the two surfaces is C_4 symmetric.

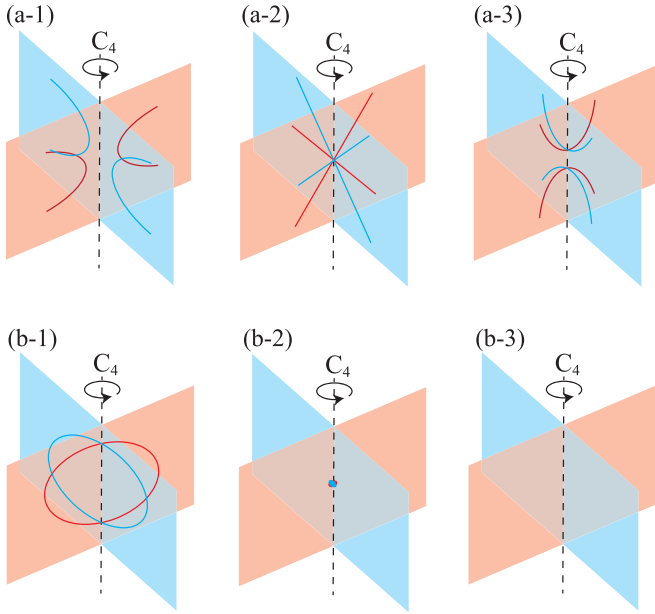


FIG. 9. Schematic pictures of the topology changes of nodal lines with the fourfold rotational symmetry in the momentum space. The red (blue) colored line represents the nodal line inside the red (blue) plane near the C_4 axis, which holds C_4 symmetry in total. There are the reconnection of the nodal lines in (a-1)–(a-3), and the annihilation (creation) of the nodal lines in (b-1)–(b-3). Away from the C_4 axis, the nodal lines may leave the blue and red planes.

Now, we apply the Morse theory in (I) and (II) separately. We obtain the gradients of the functions used in the Morse theory at a point along the C_4 axis (k_z axis):

$$\nabla_{\mathbf{k},m} f(0, 0, k_z, m) = (0, 0, 0, 1)^T, \quad (48)$$

$$\nabla_{\mathbf{k},m} a_x^{(\pm)}(0, 0, k_z, m) = (\cdot, \cdot, 0, 0)^T, \quad (49)$$

$$\nabla_{\mathbf{k},m} a_z(0, 0, k_z, m) = (0, 0, \cdot, \cdot)^T. \quad (50)$$

In case (I) [and also in case (II)], similar to the C_2 -symmetric case the critical point should satisfy $\nabla_{\mathbf{k},m} f \propto \nabla_{\mathbf{k},m} a_z$. Thus the critical point $(\mathbf{k}, m) = (0, 0, k_z, m)$ is determined by two conditions $a_z = 0$ and $\frac{\partial a_z}{\partial k_z} = 0$, and this set of equations can have solutions for two variables k_z and m . Because these conditions, $a_z = 0$ and $\frac{\partial a_z}{\partial k_z} = 0$, are common between cases (I) and (II), the critical points are common.

The resulting evolutions of nodal lines across the topology change are illustrated in Fig. 9. The normal vectors of the two surfaces $a_x^{(\pm)}(\mathbf{k}) = 0$ are given by $\nabla_{\mathbf{k}} a_x^{(\pm)}(\mathbf{k})$; hence at the critical point, they are perpendicular to each other and also perpendicular to the z axis. Evolutions of nodal lines are confined to each plane near the critical point, and they follow the C_4 symmetry in total. When $\mathcal{N} = 1$ corresponding to the reconnection, the nodal lines evolve from Figs. 9(a-1) to 9(a-3) through 9(a-2), and vice versa, which is in a good agreement with the result by the numerical calculation in Fig. 8. When $\mathcal{N} = 2$ and the annihilation happens, the nodal lines evolve from Figs. 9(b-1) to 9(b-3) through 9(b-2). Its reverse process from Figs. 9(b-3) to 9(b-1) corresponds to the creation of a nodal line with $\mathcal{N} = 0$.

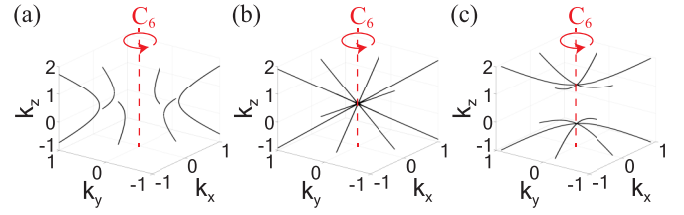


FIG. 10. Evolutions of nodal lines with the fourfold rotational symmetry in the momentum space. Nodal lines are given by the Hamiltonian $\mathcal{H}^{(C_6)}(\mathbf{k})$ with $c_1 = 1$, $c_2 = 1$, $c_3 = 0$, $c_4 = 0$, $c_5 = 1$, $c_6 = -1$, and $c_7 = 1$. (a), (b), and (c) represent nodal lines with $m = -0.75$, -0.25 , and 0.25 , respectively. The nodal lines are reconnected at $m = -0.25$ in (b).

4. C_6 symmetry

We consider nodal lines with \mathcal{PT} symmetry and sixfold rotational symmetry along the k_z axis. We discuss topology changes of nodal lines at a point $\mathbf{k} = \mathbf{k}_0$ on the C_6 axis (k_z axis). In spinless systems, the eigenvalue of C_6 is 1 for the irrep A, -1 for the irrep B, $e^{-2\pi i/3}$ for the irrep 2E_1 , $e^{\pi i/3}$ for the irrep 2E_2 , $e^{2\pi i/3}$ for the irrep 1E_1 , and $e^{-\pi i/3}$ for the irrep 1E_2 . Here, the pairs of irreps (1E_1 , 2E_1) and (1E_2 , 2E_2) form Kramers degeneracy because they are complex representations. Therefore we can restrict ourselves to the irreps A and B. We will study the case where the two bands follow the same irreps (A or B) in Sec. IV B. In this section we study the remaining case where one of the two bands follows the irrep A and the other follows the irrep B. Then, the representation matrix of the C_6 rotation is obtained as

$$D(C_6) = \begin{pmatrix} 1 & 0 \\ 0 & -1 \end{pmatrix}. \quad (51)$$

We shift the origin in \mathbf{k} space by \mathbf{k}_0 , so that the focused point becomes $\mathbf{k} = 0$.

Similar to the previous cases, we begin with a simple example; by using Eq. (34), the $\mathbf{k} \cdot \mathbf{p}$ Hamiltonian around $\mathbf{k} = 0$ is written up to the third order in \mathbf{k} as

$$\mathcal{H}^{(C_6)}(\mathbf{k}) = a_x^{(C_6)} \sigma_x + a_z^{(C_6)} \sigma_z, \quad (52)$$

$$a_x^{(C_6)}(\mathbf{k}) = c_1 k_x (k_x^2 - 3k_y^2) + c_2 k_y (k_y^2 - 3k_x^2), \quad (53)$$

$$a_z^{(C_6)}(\mathbf{k}) = c_3 k_z^3 + c_4 (k_x^2 + k_y^2) k_z + c_5 (k_x^2 + k_y^2) + c_6 k_z^2 + c_7 k_z + m, \quad (54)$$

where c_i ($i = 1, 2, \dots, 7$) and m are real parameters. We set $c_1 = 1$, $c_2 = 1$, $c_3 = 0$, $c_4 = 0$, $c_5 = 1$, $c_6 = -1$, and $c_7 = 1$ as an example. In $a_x^{(C_6)}(\mathbf{k})$ [Eq. (53)], the lowest order terms are of the third order in \mathbf{k} . On the other hand the third order terms of $a_z^{(C_6)}(\mathbf{k})$ in Eq. (54) are not essential and they are set to be zero, i.e., $c_3 = c_4 = 0$, for simplicity. With this choice of parameter values as shown in Fig. 10, nodal lines are reconnected by increasing m . Figures 10(a), 10(b) and 10(c) represent nodal lines with $m = -0.75$, -0.25 , and 0.25 , respectively. When m is changed from $m = -0.75$ to $m = 0.25$, the nodal lines are reconnected at $\mathbf{k} = (0, 0, \frac{1}{2})$ with $m = -\frac{1}{4}$.

Similar to the case with the C_4 symmetry, the topology change of nodal lines cannot be studied within the Morse

theory because $\nabla_{\mathbf{k}} a_x^{(C_6)} = 0$ there. Meanwhile, as is the same with C_4 symmetry in Sec. IV A 3, we find that the function $a_x^{(C_6)}$ can always be factorized even in general cases with C_6 symmetry, and then the topology change of nodal lines can be fully characterized by the index \mathcal{N} for critical points within the Morse theory. Then we find that the evolutions of nodal lines occur on three surfaces containing the C_6 axis, and the events such as reconnection, annihilation, and creation are confined to each surface following C_6 symmetry in total as we give detailed explanations in Appendix F.

B. Case with the two bands having the same irrep for C_n symmetry ($n = 2, 4, \text{ and } 6$)

We have considered the nodal lines with the representation matrix composed of two different irreps in C_n symmetry ($n = 2, 4, \text{ and } 6$) so far. In this section, we consider the other case where the two bands have the same irrep (A or B). The representation matrix is now written as an identity matrix:

$$D(C_n) = \pm \begin{pmatrix} 1 & 0 \\ 0 & 1 \end{pmatrix}, \quad (55)$$

where the plus and minus signs correspond to the A and B irreps, respectively. Because of Eq. (34), we obtain $a_x(\mathbf{k}) = a_x(C_n \mathbf{k})$ and $a_z(\mathbf{k}) = a_z(C_n \mathbf{k})$ as symmetry constraints.

The gradients of functions needed for the Morse theory at a point along the C_n rotational axis (k_z axis) are

$$\nabla_{\mathbf{k},m} f(0, 0, k_z, m) = (0, 0, 0, 1)^T, \quad (56)$$

$$\nabla_{\mathbf{k},m} a_x(0, 0, k_z, m) = (0, 0, \cdot, \cdot)^T, \quad (57)$$

$$\nabla_{\mathbf{k},m} a_z(0, 0, k_z, m) = (0, 0, \cdot, \cdot)^T. \quad (58)$$

When we focus on the k_z and m components because all the others are zero, the three vectors in Eqs. (56)–(58) reside in a 2D vector space. Therefore, whenever the nodal line cross the k_z axis, this crossing point $(0, 0, k_z, m)$ is always a critical point since these three vectors are linearly dependent. Therefore the orthogonal projection \mathcal{P} is given by $\mathcal{P} = \text{diag}(1, 1, 0, 0)$, i.e., a projection to the k_x - k_y plane, and the matrix \mathcal{M} is regarded as a 2×2 matrix within the k_x - k_y plane on which C_n symmetry is preserved. In the C_2 -symmetric case, the two eigenvalues of \mathcal{M} are nonzero and independent in general, and the index \mathcal{N} can have the values 0, 1, or 2. On the other hand, on the C_4 -symmetric and C_6 -symmetric cases, the matrix \mathcal{M} has the form $\mathcal{M} = \text{diag}(u, u)$, where u is a real number, due to the above symmetry constraints: $a_x(\mathbf{k}) = a_x(C_n \mathbf{k})$ and $a_z(\mathbf{k}) = a_z(C_n \mathbf{k})$. Consequently, depending on the sign of u , the index \mathcal{N} only gives 0 or 2, corresponding to the creation or the annihilation of nodal lines. In particular, in the C_4 - and C_6 - symmetric cases, reconnections of nodal lines never occur on the C_n axis.

In order to see evolutions of nodal lines under the C_n symmetry, we note that $\nabla_{\mathbf{k}} a_x(z)|_P = (0, 0, \cdot)^T$ at the critical point P on the C_n axis defines a normal vector of the surface $a_x(z) = 0$. Hence, in the vicinity of the critical point P , the nodal lines lie along the plane perpendicular to the rotational axis (k_z axis) as shown in Fig. 11. The nodal lines are illustrated as red lines inside the red plane which is perpendicular to the rotational axis. When $\mathcal{N} = 2$, the annihilation of nodal lines happens, and

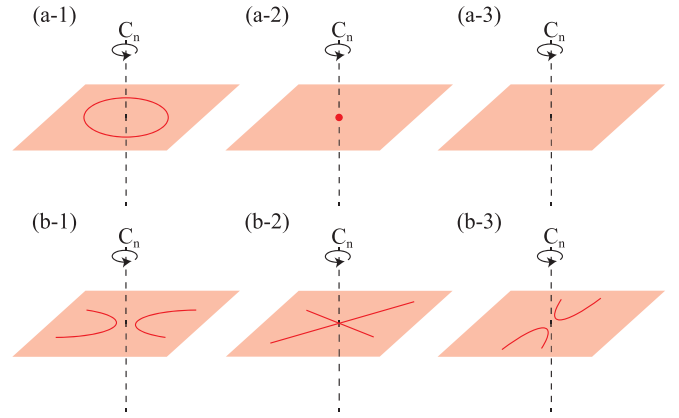


FIG. 11. Evolutions of nodal lines with the C_n symmetry ($n = 2, 4, \text{ and } 6$) in the momentum space. The red lines represent nodal lines inside the red plane which is perpendicular to the rotational axis. The annihilation (creation) of nodal lines occurs in (a-1)–(a-3) in the C_n symmetry. The reconnection of nodal lines occurs in (b-1)–(b-3) only in the C_2 symmetry, and is prohibited in the C_4 and C_6 symmetries.

the nodal lines evolve from Figs. 11(a-1) to 11(a-3) through 11(a-2). The case with $\mathcal{N} = 0$ corresponds to the creation, which is a reverse process from Figs. 11(a-3) to 11(a-1). These two processes are allowed in the C_n symmetry ($n = 2, 4, \text{ and } 6$) as we discuss in the previous paragraph. In the case with $\mathcal{N} = 1$, corresponding to the reconnection, the nodal lines evolve from Figs. 11(b-1) to 11(b-3) through 11(b-2). This process is allowed only in systems with C_2 symmetry but not with C_4 or C_6 symmetry. This is naturally understood graphically; by drawing the figures similar to Figs. 11(b-1)–11(b-3) for C_n ($n = 4$ and 6), one can see that it is improbable for the n nodal lines to meet at the C_n axis. To summarize, when the irreps of the C_n symmetry ($n = 2, 4, \text{ and } 6$) for the conduction and the valence bands are the same, the creation and the annihilation of nodal lines are allowed, but only the C_2 symmetry allows nodal lines to reconnect on the C_n axis.

C. Cases with mirror symmetry

In this section, we consider nodal lines with \mathcal{PT} symmetry and mirror symmetry M_z with respect to the xy plane. In spinless systems, the eigenvalue of M_z is 1 for the irrep A' and -1 for the irrep A'' . We discuss topology changes of nodal lines on the mirror-invariant plane. Since the two mirror-invariant planes $k_z = 0$ and $k_z = \pi$ can be studied similarly, we focus on the $k_z = 0$ plane here. In this section, we consider the case where one of the two bands follows the irrep A' and the other follows the irrep A'' . The other case with the two bands following the same irrep (A' or A'') will be discussed in Sec. IV D. Then, the representation matrix of the mirror operation is

$$D(M_z) = \begin{pmatrix} 1 & 0 \\ 0 & -1 \end{pmatrix}. \quad (59)$$

We focus on a point \mathbf{k}_0 on the mirror plane, and we shift the origin to the point \mathbf{k}_0 for simplicity. By using Eq. (34), we obtain $a_x(k_x, k_y, -k_z) = -a_x(k_x, k_y, k_z)$ and $a_z(k_x, k_y, -k_z) =$

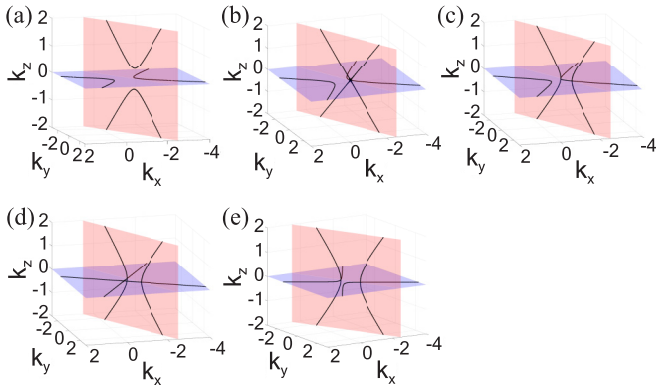


FIG. 12. Evolutions of nodal lines with the mirror symmetry in the momentum space, when the two bands have the opposite mirror eigenvalues. Nodal lines are given by the Hamiltonian $\mathcal{H}^{(M_z)}(\mathbf{k})$ with $c_1 = 1, c_2 = \frac{1}{2}, c_3 = 1, c_4 = 1, c_5 = -1, c_6 = 1, c_7 = 1, c_8 = 1,$ and $c_9 = 1$. (a), (b), (c), (d), and (e) represent nodal lines with $m = -0.2, -0.05, 0.1, 0.2,$ and 0.3 , respectively. The blue plane is $k_z = 0$ plane. The nodal lines are reconnected at $m = -0.05$ and $m = 0.2$ on the red plane and the blue plane in (b) and (d), respectively.

$a_z(k_x, k_y, k_z)$. Thus the $\mathbf{k} \cdot \mathbf{p}$ Hamiltonian around $\mathbf{k} = 0$ reflecting M_z symmetry is written up to the second order in \mathbf{k} as

$$\mathcal{H}^{(M_z)}(\mathbf{k}) = a_x^{(M_z)}\sigma_x + a_z^{(M_z)}\sigma_z, \quad (60)$$

$$a_x^{(M_z)}(\mathbf{k}) = c_1 k_x k_z + c_2 k_y k_z + c_3 k_z, \quad (61)$$

$$a_z^{(M_z)}(\mathbf{k}) = c_4 k_x^2 + c_5 k_y^2 + c_6 k_z^2 + c_7 k_x k_y + c_8 k_x + c_9 k_y + m, \quad (62)$$

where c_i ($i = 1, 2, \dots, 9$) and m are real parameters. We set $c_1 = 1, c_2 = \frac{1}{2}, c_3 = 1, c_4 = 1, c_5 = -1, c_6 = 1, c_7 = 1, c_8 = 1,$ and $c_9 = 1$ as an example. Figures 12(a), 12(b), 12(c), 12(d), and 12(e) represent nodal lines with $m = -0.2, -0.05, 0.1, 0.2,$ and 0.3 , respectively, and the blue plane is the $k_z = 0$ plane. When m is changed from $m = -0.2$ to $m = 0.1$, the nodal lines outside of the mirror plane ($k_z = 0$) meet each other at $\mathbf{k} = (-\frac{11}{10}, \frac{1}{5}, 0)$ with $m = -0.05$, and they are reconnected [Fig. 12(b)]. At this reconnection, another nodal line on this mirror plane $k_z = 0$ also crosses this critical point. Moreover, when m is changed from $m = 0.1$ to $m = 0.3$, the nodal lines on the mirror plane $k_z = 0$ are reconnected at $\mathbf{k} = (-\frac{3}{5}, \frac{1}{5}, 0)$ with $m = 0.2$ [Fig. 12(d)].

We now explain the reason why there are two types of reconnections, by noting that $a_x^{(M_z)}(\mathbf{k})$ can be factorized:

$$a_x^{(M_z)}(\mathbf{k}) = k_z \left(k_x + \frac{1}{2} k_y + 1 \right) \equiv k_z \tilde{a}_x^{(M_z)}(\mathbf{k}), \quad (63)$$

where $\tilde{a}_x^{(M_z)}(\mathbf{k}) = k_x + \frac{1}{2} k_y + 1$. Therefore the condition for nodal lines is decomposed into two cases

- (I) $k_z = 0$ and $a_z^{(M_z)}(\mathbf{k}) = 0$,
- (II) $\tilde{a}_x^{(M_z)}(\mathbf{k}) = 0$ and $a_z^{(M_z)}(\mathbf{k}) = 0$.

In case (I), two nodal lines on the mirror plane ($k_z = 0$) meet and reconnect. It occurs at $(\mathbf{k}, m) = (-\frac{3}{5}, \frac{1}{5}, 0, \frac{1}{5})$ with

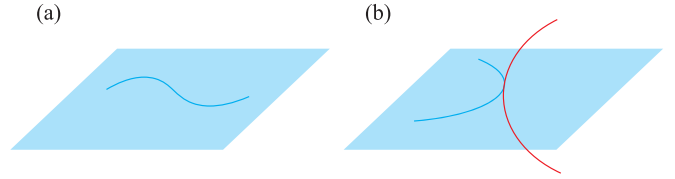


FIG. 13. Schematic pictures of existence of nodal lines with the mirror symmetry in the momentum space, when the two bands have the opposite mirror eigenvalues. (a) The blue line represents the nodal line inside the mirror plane which is illustrated as blue plane. (b) The red line is the nodal line outside the mirror plane.

index $\mathcal{N} = 1$ by the Kamiya theorem corresponding to Fig. 12(d). On the other hand, case (II) describes nodal lines outside of the mirror plane, and at the critical point they meet on the mirror plane $k_z = 0$. Therefore, at this point, another nodal line in case (I) lying on the mirror plane also goes across the critical point [see Fig. 12(b)]. It occurs at $(\mathbf{k}, m) = (-\frac{11}{10}, \frac{1}{5}, 0, -\frac{1}{20})$ with index $\mathcal{N} = 1$, corresponding to the reconnection.

Thus we show that there are two types of nodal-line reconnections from the model (60)–(62). We can show that also in general systems with mirror symmetry, there are two types, (I) and (II), of topology changes of nodal lines from the Morse theory. Let us assume that $a_x(\mathbf{k})$ and $a_z(\mathbf{k})$ are general analytic functions of \mathbf{k} under the M_z symmetry. Even so, $a_x(\mathbf{k})$ is factorized:

$$a_x(\mathbf{k}) = k_z \tilde{a}_x(\mathbf{k}), \quad (64)$$

where $\tilde{a}_x(\mathbf{k})$ is an analytic function of \mathbf{k} satisfying $\tilde{a}_x(k_x, k_y, -k_z) = \tilde{a}_x(k_x, k_y, k_z)$. The condition for the nodal line is divided into two cases due to the factorization as follows:

- (I) $k_z = 0$ and $a_z(\mathbf{k}) = 0$,
- (II) $\tilde{a}_x(\mathbf{k}) = 0$ and $a_z(\mathbf{k}) = 0$.

In cases (I) and (II), the nodal lines appear inside the mirror plane and outside the mirror plane, and they are illustrated as the blue lines on the mirror plane (blue plane) and the red lines outside the mirror plane in Fig. 13, respectively. In case (I), the nodal line exists on the mirror plane as shown in Fig. 13(a). Meanwhile, in case (II) where the nodal line exists outside the mirror plane, when the nodal line meets the mirror plane as shown in Fig. 13(b), the condition of case (I) is also satisfied there, and it connects with another nodal line on the mirror plane.

We now classify the critical points in terms of the Morse theory. We obtain the gradients of the functions needed for the Morse theory on the mirror plane ($k_z = 0$):

$$\nabla_{\mathbf{k}, m} f(k_x, k_y, 0, m) = (0, 0, 0, 1)^T, \quad (65)$$

$$\nabla_{\mathbf{k}, m} \tilde{a}_x(k_x, k_y, 0, m) = (\cdot, \cdot, 0, \cdot)^T, \quad (66)$$

$$\nabla_{\mathbf{k}, m} a_z(k_x, k_y, 0, m) = (\cdot, \cdot, 0, \cdot)^T. \quad (67)$$

In case (I), the function \tilde{a}_x is not involved, and Eqs. (65) and (67) should be linearly dependent at the critical point, and it holds when $\partial_{k_x} a_z = 0$ and $\partial_{k_y} a_z = 0$ are satisfied. Therefore the number of the conditions (i.e., $\partial_{k_x} a_z = 0, \partial_{k_y} a_z = 0, a_z = 0$) is three, and it is equal to the number of variables for

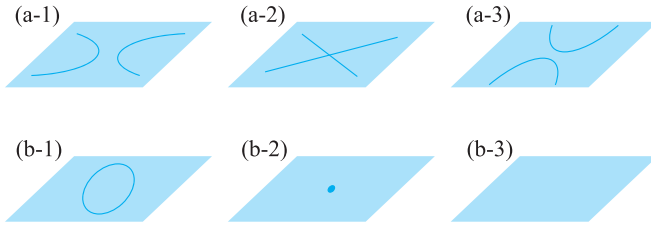


FIG. 14. Schematic pictures of evolution of nodal lines inside the mirror plane in the momentum space [case (I)], when the two bands have the opposite mirror eigenvalues. The blue colored lines represent nodal line inside mirror plane, which is illustrated as the blue plane. The reconnection of nodal lines happens in (a-1)–(a-3), and the annihilation (creation) does in (b-1)–(b-3).

$(\mathbf{k}, m) = (k_x, k_y, 0, m)$. This is illustrated as the crossing point on the blue plane in Fig. 12(d). On the other hand, in case (II), if there is a point $(k_x, k_y, 0, m)$ satisfying

$$\text{Det} \begin{pmatrix} \partial_{k_x} \tilde{a}_x & \partial_{k_x} a_z \\ \partial_{k_y} \tilde{a}_x & \partial_{k_y} a_z \end{pmatrix} = 0, \quad (68)$$

that point is regarded as a critical point because $\nabla_{\mathbf{k},m} f = \alpha_x \nabla_{\mathbf{k},m} \tilde{a}_x + \alpha_z \nabla_{\mathbf{k},m} a_z$ is satisfied for real parameters α_x and α_z . The critical point can exist because the number of conditions [i.e., Eq. (68), $\tilde{a}_x = 0$, and $a_z = 0$] is three, and it is the same with the number of variables for $(\mathbf{k}, m) = (k_x, k_y, 0, m)$. The crossing point on the red plane in Fig. 12(b) is an example of the above discussion.

We now discuss topology changes of nodal lines for cases (I) and (II) separately. In case (I), the nodal lines inside the mirror plane evolve as Fig. 14. When $\mathcal{N} = 1$, the nodal lines are reconnected, and they evolve as Figs. 14(a-1) to 14(a-3) through 14(a-2). These figures match with the reconnection of nodal lines on the blue plane in Figs. 12(c), 12(d) and 12(e). When $\mathcal{N} = 2$ and the annihilation happens, the nodal lines evolve from Figs. 14(b-1) to 14(b-3) through 14(b-2). Its reverse process is the creation with $\mathcal{N} = 0$, where the nodal ring shrinks to a point on the mirror plane. Next, in case (II), the nodal lines outside the mirror plane (red lines in Fig. 15) evolve from 15(a-1) to 15(a-3) through 15(a-2),

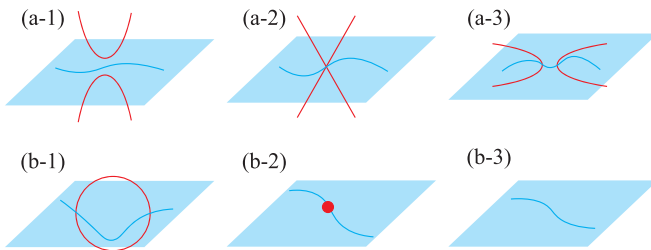


FIG. 15. Schematic pictures of evolution of nodal lines outside the mirror plane in the momentum space [case (II)], when the two bands have the opposite mirror eigenvalues. The blue lines represent nodal lines inside the mirror plane which is illustrated as blue plane, and the red lines are described as nodal lines outside the mirror plane. When the red colored nodal lines penetrate the mirror plane, they touch with blue colored nodal lines. The reconnection of the nodal lines occurs in (a-1)–(a-3), and the annihilation (creation) of the nodal lines occurs in (b-1)–(b-3).

and vice versa when the reconnection happens, corresponding to $\mathcal{N} = 1$. Particularly, in Figs. 15(a-2) and 15(a-3), the red colored nodal lines cross the blue colored nodal line on the mirror plane because they penetrate mirror plane. These figures explain the reconnection on the red plane in Figs. 12(a), 12(b) and 12(c). When $\mathcal{N} = 2$ and the annihilation happens, the nodal lines evolve from Figs. 15(b-1) to 15(b-3) through 15(b-2). Its reverse process is the creation with $\mathcal{N} = 0$, where the nodal ring shrinks to a point on the mirror plane because of the mirror symmetry.

D. Case with two bands having the same irrep for mirror symmetry

In this section, we consider the case where the two bands have the same irrep (A' or A'') in mirror symmetric systems. The representation matrix is written as

$$D(M_z) = \pm \begin{pmatrix} 1 & 0 \\ 0 & 1 \end{pmatrix}, \quad (69)$$

where the plus and minus signs correspond to A' and A'' irreps, respectively. and we obtain $a_x(\mathbf{k}) = a_x(M_z \mathbf{k})$ and $a_z(\mathbf{k}) = a_z(M_z \mathbf{k})$ because of Eq. (34).

The gradients of the functions needed for the Morse theory at a point on the mirror plane ($k_z = 0$) are

$$\nabla_{\mathbf{k},m} f(k_x, k_y, 0, m) = (0, 0, 0, 1)^T, \quad (70)$$

$$\nabla_{\mathbf{k},m} a_x(k_x, k_y, 0, m) = (\cdot, \cdot, 0, \cdot)^T, \quad (71)$$

$$\nabla_{\mathbf{k},m} a_z(k_x, k_y, 0, m) = (\cdot, \cdot, 0, \cdot)^T. \quad (72)$$

If there is a point $(k_x, k_y, 0, m)$ satisfying

$$\text{Det} \begin{pmatrix} \partial_{k_x} a_x & \partial_{k_x} a_z \\ \partial_{k_y} a_x & \partial_{k_y} a_z \end{pmatrix} = 0, \quad (73)$$

the point is a critical point because $\nabla_{\mathbf{k},m} f = \alpha_x \nabla_{\mathbf{k},m} a_x + \alpha_z \nabla_{\mathbf{k},m} a_z$ is satisfied for real parameters α_x and α_z . The critical point is determined by three conditions [i.e., Eq (73), $a_x = 0$, and $a_z = 0$], and these equations can have solutions for three variables (i.e., k_x , k_y , and m). Then, the eigenvalues of the 2×2 matrix \mathcal{M} are nonzero in general, and the critical point is characterized by the index \mathcal{N} into three cases, $\mathcal{N} = 0, 1, 2$, corresponding to creation, reconnection, and annihilation of nodal lines, respectively.

In order to see topology changes of nodal lines under the mirror symmetry, we note that the normal vector of the surface $a_i = 0$ ($i = x, z$) at any point on the mirror plane is parallel to $\nabla_{\mathbf{k}} a_i|_P = (\cdot, \cdot, 0)^T$. Thus the tangent vector of the nodal line at any point on the mirror plane is $\mathbf{t} \parallel \nabla_{\mathbf{k}} a_x \times \nabla_{\mathbf{k}} a_z \parallel (0, 0, 1)$, and it is always perpendicular to the mirror plane as shown in Fig. 16. (Note that at a critical point, $\nabla_{\mathbf{k}} a_x$ and $\nabla_{\mathbf{k}} a_z$ are parallel due to Eq. (73), and the tangent vector \mathbf{t} cannot be determined, as is naturally expected.) The red lines represent nodal lines outside the mirror plane which is colored by blue. When $\mathcal{N} = 1$, the reconnection of nodal lines occurs, and the nodal lines evolve from Figs. 16(a-1) to 16(a-3) through 16(a-2) and vice versa. When $\mathcal{N} = 2$ corresponding to the annihilation, the nodal line evolves from Figs. 16(b-1) to 16(b-3) through 16(b-2). In the case with $\mathcal{N} = 0$, the nodal line is created as a reverse process of the annihilation.

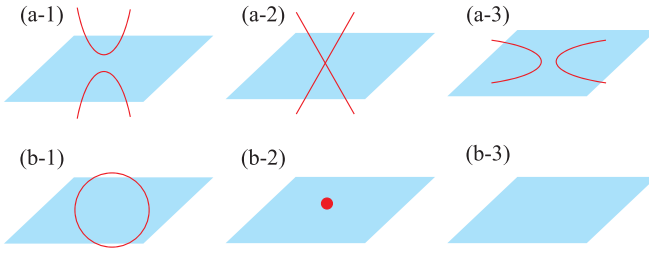


FIG. 16. Schematic pictures of evolution of nodal lines outside the mirror plane in the momentum space, when the two bands have the same mirror eigenvalues. The red lines are described as nodal lines outside the mirror plane illustrated as blue plane. The reconnection of the nodal lines occurs in (a-1)–(a-3), and the annihilation (creation) of the nodal lines occurs in (b-1)–(b-3).

V. SUMMARY

In this paper, we reveal that there are three types of evolutions of nodal lines with PT symmetry such as the creation, reconnection, and annihilation. Such topology changes of nodal lines are understood by the local maximum, the saddle point, or the local minimum of the function $f(\mathbf{k}, m) = m$ in the 4D (\mathbf{k}, m) space. These critical points are characterized by the index $\mathcal{N} = 0, 1,$ and 2 corresponding to the creation, reconnection, and annihilation in the Morse theory, and we give examples for the transition of nodal lines. As a result, we show that a phase transition between the nodal lines and the nodal link cannot occur directly, but via several reconnections of nodal lines, if no additional crystallographic symmetries are assumed.

Moreover we extend our theory to the case with the rotational symmetries and the mirror symmetry, and disclose the possible topology changes of nodal lines. When the system has C_n symmetry ($n = 2, 4,$ and 6), the events of topology changes of nodal lines occur inside the plane containing (perpendicular to) the C_n axis with the different (the same) irreps for the two band. We exclude the C_3 symmetric case because the nodal line always lies along the rotational axis. When the two bands have different irreps with C_n symmetry ($n = 2, 4,$ and 6), all events for the topology changes of nodal lines (i.e., creation, reconnection, and annihilation) are possible. Meanwhile, with the same irreps for the two bands, only creation and annihilation are allowed in $n = 4$ and 6 because of the symmetry constraints, whereas all events are allowed on $n = 2$. When the system has the mirror symmetry with two bands having the different irreps, the topology changes of nodal lines classified into those for nodal lines inside and outside of the mirror plane, corresponding to cases (I) and (II) in Sec. IV C, respectively. On the other hand, if the two bands have the same irreps, the nodal lines reside only outside the mirror plane, and can experience all possible topology changes.

Thus we have shown that the topology changes of nodal lines are determined by the point-group symmetry of the \mathbf{k} point at which the topology change occurs. In this paper, we limit ourselves to the simplest point groups such as rotation or mirror reflection only. An extension to other point groups is beyond of this paper, and is left as a future work. In this paper, we limit ourselves to the nodal lines composed of one

conduction band and one valence band, and we describe the nodal lines in terms of the two-band model. It should be interesting if we extend our analysis to the cases with the larger number of bands, which will include various intriguing cases such as the triple points [59] and double band inversion [60]. Nonetheless, the analysis for the larger number of bands will be largely different and much more complicated than the two-band cases. Therefore the extension to multiband systems is left for future work.

ACKNOWLEDGMENT

This work is supported by JSPS KAKENHI Grants No. JP20J23473, No. JP22K18687, and No. JP22H00108.

APPENDIX A: KAMIYA THEOREM

The nodal lines evolve by changing the parameter m , and all possible nodal lines configure the manifold M in (\mathbf{k}, m) space. The topology changes of nodal lines occur across the critical points on the manifold M . To identify the local structure of the manifold M around the critical points, we adopt the Kamiya theorem in Secs. III and IV. In this Appendix, we explain the Kamiya theorem.

The Kamiya theorem is as follows [56]. Let M be a differentiable function described as

$$M = \{Q \in \mathbb{R}^n | f_1(Q) = \cdots = f_r(Q) = 0\}, \quad (\text{A1})$$

where $f_1, \dots, f_r : \mathbb{R}^n \rightarrow \mathbb{R}$ are differentiable functions, and $\nabla f_1(Q), \dots, \nabla f_r(Q)$ be linearly independent. If and only if for a given function $f : \mathbb{R}^n \rightarrow \mathbb{R}$, the following equation holds

$$\nabla f(Q_0) = a_1 \nabla f_1(Q_0) + \cdots + a_r \nabla f_r(Q_0) \quad a_i \in \mathbb{R}, \quad (\text{A2})$$

$Q_0 \in M$ is a critical point of the function $\bar{f} = f|_M : M \rightarrow \mathbb{R}$. Then, let $Q_0 \in M$ be a critical point of \bar{f} , and \mathcal{P} be a orthogonal projection from \mathbb{R}^n to a tangent vector space $T_{Q_0}(M)$ at Q_0 , i.e., $\mathcal{P} : \mathbb{R}^n \rightarrow T_{Q_0}(M)$. If and only if a rank of a matrix

$$\mathcal{M} = \mathcal{P}(\mathcal{H}(f)|_{Q_0}) - \sum_{i=1}^r a_i \mathcal{H}(f_i)|_{Q_0} \mathcal{P}, \quad (\text{A3})$$

where \mathcal{H} is a Hessian matrix, is $n - r$, i.e., rank $\mathcal{M} = n - r$, the critical point Q_0 is nondegenerate. Moreover, an index of f at Q_0 is equal to the number of negative eigenvalues of matrix \mathcal{M} . In the main text, we take $n = 4$, $r = 2$, $f_1 = a_x$, and $f_2 = a_z$.

APPENDIX B: MORSE LEMMA

The Morse lemma [54,55] used in Secs. III and IV tells us the local shape of the function f near its critical point. Let M be a differentiable function and $f : M \rightarrow \mathbb{R}$ be a differentiable function. When a point $Q \in M$ is a nondegenerate critical point of f , the function f can be expressed in terms of a local coordinate $(U; x_1, \dots, x_n)$ around Q :

$$x_1(Q) = \cdots = x_n(Q) = 0, \quad (\text{B1})$$

$$f = f(Q) - x_1^2 - \cdots - x_r^2 + x_{r+1}^2 + \cdots + x_n^2, \quad (\text{B2})$$

where r is a index of f on Q .

APPENDIX C: DETAILED CALCULATION FOR THE INDEX OF THE ANNIHILATION CASE

We show the detailed calculations of the model for the annihilation. As the gradients of $a_j^{(C)}(\mathbf{k}, m)$ for $j = x, z$ at $(\mathbf{k}, m) = (0, 0)$ are

$$\nabla_{\mathbf{k}, m} a_x^{(C)}(0, 0) = \begin{pmatrix} 1 \\ 0 \\ 0 \\ 2 \end{pmatrix}, \quad \nabla_{\mathbf{k}, m} a_z^{(C)}(0, 0) = \begin{pmatrix} 1 \\ 0 \\ 0 \\ 1 \end{pmatrix}, \quad (\text{C1})$$

we get the following relationship:

$$\nabla_{\mathbf{k}, m} f(0, 0) = \nabla_{\mathbf{k}, m} a_x^{(C)}(0, 0) - \nabla_{\mathbf{k}, m} a_z^{(C)}(0, 0). \quad (\text{C2})$$

This equation implies that $Q(0, 0)$ is a critical point by the Kamiya theorem. The vectors in Eq. (C1) span a 2D vector space with basis vectors

$$\mathbf{b}_1^{(C)} = \begin{pmatrix} 1 \\ 0 \\ 0 \\ 0 \end{pmatrix}, \quad \mathbf{b}_2^{(C)} = \begin{pmatrix} 0 \\ 0 \\ 0 \\ 1 \end{pmatrix}, \quad (\text{C3})$$

and an orthogonal projection to a tangent vector space at the critical point $Q(0, 0)$ is written as

$$\mathcal{P}^{(C)} = I_4 - \mathbf{b}_1^{(C)} \mathbf{b}_1^{(C)T} - \mathbf{b}_2^{(C)} \mathbf{b}_2^{(C)T} \quad (\text{C4})$$

$$= \begin{pmatrix} 0 & & & \\ & 1 & & \\ & & 1 & \\ & & & 0 \end{pmatrix}. \quad (\text{C5})$$

Moreover Hessian matrices of $a_j^{(C)}(\mathbf{k}, m)$ and $f(\mathbf{k}, m)$ at the critical point Q are obtained as

$$\mathcal{H}(a_x^{(C)})|_Q = \begin{pmatrix} 1 & & & \\ & 2 & & \\ & & 2 & \\ & & & 1 \end{pmatrix}, \quad (\text{C6})$$

$$\mathcal{H}(a_z^{(C)})|_Q = \begin{pmatrix} -1 & & & \\ & 1 & & \\ & & -1 & \\ & & & -1 \end{pmatrix}, \quad (\text{C7})$$

$$\mathcal{H}(f)|_Q = 0. \quad (\text{C8})$$

A matrix $\mathcal{M}^{(C)}$ written as

$$\begin{aligned} \mathcal{M}^{(C)} &= \mathcal{P}^{(C)} (\mathcal{H}(f)|_Q - \mathcal{H}(a_x^{(C)})|_Q + \mathcal{H}(a_z^{(C)})|_Q) \mathcal{P}^{(C)} \\ &= \begin{pmatrix} 0 & & & \\ & -1 & & \\ & & -3 & \\ & & & 0 \end{pmatrix} \end{aligned} \quad (\text{C9})$$

indicates that the critical point Q is nondegenerate by the Kamiya theorem because the rank of $\mathcal{M}^{(C)}$ is 2. Furthermore, as the number of the negative eigenvalues is equal to an index of f at the critical point Q , the index \mathcal{N} of $f(Q)$ is 2.

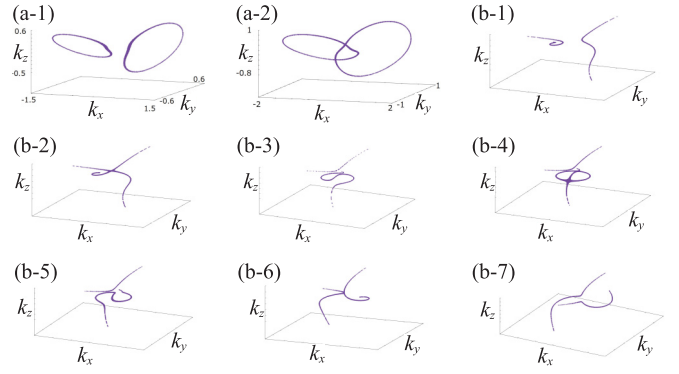


FIG. 17. Nodal lines in the Hamiltonian $\mathcal{H}^{(A)}$ with an additional term. There are two nodal lines with $m = 3.2$ in (a-1) and there is the nodal link with $m = 2.8$ in (a-2). The intermediate states between the nodal lines and the nodal link are illustrated in (b-1)–(b-7) as enlarged views. The nodal lines with $m = 3.07, 3.05, 3, 2.995, 2.99, 2.95,$ and 2.93 are illustrated in (b-1)–(b-7) in this order. From the two nodal lines to a nodal link, reconnections occur three times in (b-2), (b-4), and (b-6).

APPENDIX D: FURTHER EXPLANATIONS FOR THE NODAL LINK

As we discussed in Sec. II B, the model (2)–(4) gives a direct phase transition between the nodal lines and the nodal link, but in terms of the Morse theory it is an artifact of the special choice of the model. Namely, $\nabla_{\mathbf{k}} a_x^{(A)} = \nabla_{\mathbf{k}} a_z^{(A)} = 0$ holds at the transition where the two nodal lines touch, but these equations cannot hold simultaneously in general, and they hold just by accident. To remove this artifact, we add some terms to the Hamiltonian: $a_x^{(A)} \rightarrow a_x^{\prime(A)} = a_x^{(A)} + \alpha \sin k_x$ and $a_z^{(A)} \rightarrow a_z^{\prime(A)} = a_z^{(A)} + \alpha \sin k_z$, where α is a real parameter. This model has the nodal lines with $m = 3.2$ and the nodal link with $m = 2.8$ in Figs. 17(a-1) and 17(a-2) like the original model $\mathcal{H}^{(A)}$. However, the intermediate states are different from the original model as shown in Figs. 17(b-1)–17(b-7), where the nodal lines with $m = 3.07, 3.05, 3, 2.995, 2.99, 2.95,$ and 2.93 are illustrated. The nodal lines are reconnected three times in Figs. 17(b-2), 17(b-4), and 17(b-6). Therefore this model requires the reconnections of nodal lines three times to get the nodal link from two nodal lines.

Thus the phase transition from two nodal lines to a nodal link cannot occur directly but via several reconnections. We show its simplest pattern schematically in Fig. 18 from (a) to (e) as an example. In this example, the nodal lines are reconnected twice between (a) and (b), and (c) and (d), and then the nodal link is finally obtained.

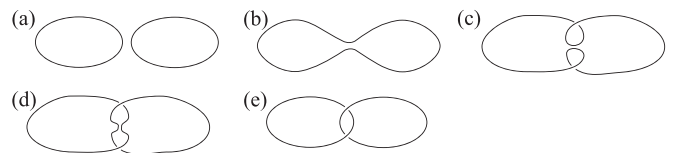


FIG. 18. Schematic pictures of evolution from the nodal lines in (a) to the nodal link (e). The reconnections happen twice as from (a) to (b) and from (c) to (d).

APPENDIX E: FACTORIZATION OF a_x

Here, we show that a_x is always factorized when the two bands have different irreps for C_4 and C_6 symmetries, as briefly explained in Secs. IV A 3 and 4. On the premise that $a_x(\mathbf{k})$ is an analytic function of k_x and k_y , one can write

$$a_x(\mathbf{k}) = \sum_{m=0}^{\infty} \sum_{n=0}^{\infty} c_{mn} k_+^m k_-^n, \quad (\text{E1})$$

where c_{mn} is a complex analytic function of k_z , and $k_{\pm} = k_x \pm ik_y$. For the following calculations, we note that $c_{nm} = \bar{c}_{mn}$ since $a_x(\mathbf{k})$ is real.

1. C_4 symmetry

When the system has C_4 symmetry, we obtain $a_x(k_+, k_-) = -a(ik_+, -ik_-)$ because of Eq. (34), and the summation in $a_x(\mathbf{k})$ is rewritten as

$$\begin{aligned} a_x(\mathbf{k}) &= \sum_{\substack{m \geq 0 \\ n \geq 0 \\ m-n \equiv 2 \pmod{4}}} c_{mn} k_+^m k_-^n, \\ &= \left(\sum_{\substack{m > n \geq 0 \\ m-n \equiv 2 \pmod{4}}} + \sum_{\substack{n > m \geq 0 \\ m-n \equiv 2 \pmod{4}}} \right) c_{mn} k_+^m k_-^n, \\ &= c_{20} k_+^2 \sum_{\substack{p=0 \\ q=0}}^{\infty} d_{pq} (k_+ k_-)^p k_+^{4q} + c_{02} k_-^2 \sum_{\substack{p=0 \\ q=0}}^{\infty} \bar{d}_{pq} (k_+ k_-)^p k_-^{4q}, \end{aligned} \quad (\text{E2})$$

where $d_{pq} = c_{p+4q+2,p}/c_{20}$. Because $d_{00} = 1$, a square root of the sum $\sum_{p=0}^{\infty} d_{pq} (k_+ k_-)^p k_+^{4q}$ is analytic in k_+ and k_- , and we can write $g^2(\mathbf{k}) = \sum_{p=0}^{\infty} d_{pq} (k_+ k_-)^p k_+^{4q}$, where $g(\mathbf{k})$ is analytic and $g(\mathbf{k} = 0) = 1$. When we introduce $i\alpha^2 = c_{20}$, where α is complex constant, $a_x(\mathbf{k})$ is explicitly factorized as follows:

$$\begin{aligned} a_x(\mathbf{k}) &= i\alpha^2 k_+^2 g^2(\mathbf{k}) - i\bar{\alpha}^2 k_-^2 \bar{g}^2(\mathbf{k}) \\ &= i(\alpha k_+ g(\mathbf{k}) - \bar{\alpha} k_- \bar{g}(\mathbf{k}))(\alpha k_+ g(\mathbf{k}) + \bar{\alpha} k_- \bar{g}(\mathbf{k})). \end{aligned} \quad (\text{E3})$$

Because $g(\mathbf{k})$ is written as $g(\mathbf{k}) = \sum_{p=0}^{\infty} f_{pq} (k_+ k_-)^p k_+^{4q}$, where f_{pq} is a complex constant, we get $g(\mathbf{k}) = g(C_4 \mathbf{k})$.

2. C_6 symmetry

When the system has C_6 symmetry, we obtain $a_x(k_+, k_-) = -a_x(e^{\frac{\pi i}{3}} k_+, e^{-\frac{\pi i}{3}} k_-)$ due to Eq. (34). Therefore, as well as the C_4 -symmetric case, $a_x(\mathbf{k})$ is factorized:

$$\begin{aligned} a_x(\mathbf{k}) &= i\alpha^3 k_+^3 g^3(\mathbf{k}) - i\bar{\alpha}^3 k_-^3 \bar{g}^3(\mathbf{k}), \\ &= i(\alpha k_+ g(\mathbf{k}) - \bar{\alpha} k_- \bar{g}(\mathbf{k})) \\ &\quad \times (\alpha k_+ e^{\frac{2}{3}\pi i} g(\mathbf{k}) - \bar{\alpha} k_- e^{-\frac{2}{3}\pi i} \bar{g}(\mathbf{k})) \\ &\quad \times (\alpha k_+ e^{\frac{4}{3}\pi i} g(\mathbf{k}) - \bar{\alpha} k_- e^{-\frac{4}{3}\pi i} \bar{g}(\mathbf{k})), \end{aligned} \quad (\text{E4})$$

where α is a complex constant, $g(\mathbf{k})$ is an analytic function of k_x and k_y with $g(\mathbf{k} = 0) = 1$, and $g(\mathbf{k}) = g(C_6 \mathbf{k})$.

APPENDIX F: DETAIL EXPLANATION UNDER C_6 SYMMETRY

In this Appendix, we show the details of the factorization of $a_x^{(C_6)}$ under C_6 symmetry, similar to the cases under C_4 symmetry. In order to study the topology change of nodal lines within the Morse theory, we will show that $a_x^{(C_6)}$ can be factorized because of the C_6 symmetry. For example, when $a_x^{(C_6)}$ is given by Eq. (54) with $c_1 = 1$ and $c_2 = 1$, it is factorized as

$$\begin{aligned} a_x^{(C_6)}(\mathbf{k}) &= (k_x + k_y)((2 - \sqrt{3})k_x - k_y)((2 + \sqrt{3})k_x - k_y) \\ &\equiv a_x^{(C_6)(\text{I})}(\mathbf{k}) a_x^{(C_6)(\text{II})}(\mathbf{k}) a_x^{(C_6)(\text{III})}(\mathbf{k}), \end{aligned} \quad (\text{F1})$$

where $a_x^{(C_6)(\text{I})}(\mathbf{k}) = k_x + k_y$, $a_x^{(C_6)(\text{II})}(\mathbf{k}) = (2 - \sqrt{3})k_x - k_y$, and $a_x^{(C_6)(\text{III})}(\mathbf{k}) = (2 + \sqrt{3})k_x - k_y$. Therefore the condition for nodal lines is decomposed into three cases:

- (I) $a_x^{(C_6)(\text{I})}(\mathbf{k}) = 0$ and $a_z^{(C_6)}(\mathbf{k}) = 0$,
- (II) $a_x^{(C_6)(\text{II})}(\mathbf{k}) = 0$ and $a_z^{(C_6)}(\mathbf{k}) = 0$,
- (III) $a_x^{(C_6)(\text{III})}(\mathbf{k}) = 0$ and $a_z^{(C_6)}(\mathbf{k}) = 0$.

In all three cases (I), (II), and (III), one can check that the point $(\mathbf{k}, m) = (0, 0, \frac{1}{2}, -\frac{1}{4})$ is a critical point with the index $\mathcal{N} = 1$ by the Kamiya theorem. Then the reconections of nodal lines on the three planes $a_x^{(C_6)(\text{I})}(\mathbf{k}) = k_x + k_y = 0$, $a_x^{(C_6)(\text{II})}(\mathbf{k}) = (2 - \sqrt{3})k_x - k_y = 0$, and $a_x^{(C_6)(\text{III})}(\mathbf{k}) = (2 + \sqrt{3})k_x - k_y = 0$ occur simultaneously by the Morse lemma in a C_6 -symmetric manner.

Apart from the above example, even when $a_x(\mathbf{k})$ and $a_z(\mathbf{k})$ are general analytic functions around the critical point $(0, 0, k_z^{(0)})$ in \mathbf{k} with the higher order terms in \mathbf{k} , we can show that $a_x(\mathbf{k})$ is factorized:

$$\begin{aligned} a_x(\mathbf{k}) &= i(\alpha k_+ g(\mathbf{k}) - \bar{\alpha} k_- \bar{g}(\mathbf{k})) \\ &\quad \times (\alpha k_+ e^{\frac{2}{3}\pi i} g(\mathbf{k}) - \bar{\alpha} k_- e^{-\frac{2}{3}\pi i} \bar{g}(\mathbf{k})) \\ &\quad \times (\alpha k_+ e^{\frac{4}{3}\pi i} g(\mathbf{k}) - \bar{\alpha} k_- e^{-\frac{4}{3}\pi i} \bar{g}(\mathbf{k})) \\ &\equiv i a_x^{(\text{I})}(\mathbf{k}) a_x^{(\text{II})}(\mathbf{k}) a_x^{(\text{III})}(\mathbf{k}), \end{aligned} \quad (\text{F2})$$

where $a_x^{(\text{I})}(\mathbf{k}) = \alpha k_+ g(\mathbf{k}) - \bar{\alpha} k_- \bar{g}(\mathbf{k})$, $a_x^{(\text{II})}(\mathbf{k}) = \alpha k_+ e^{\frac{2}{3}\pi i} g(\mathbf{k}) - \bar{\alpha} k_- e^{-\frac{2}{3}\pi i} \bar{g}(\mathbf{k})$, $a_x^{(\text{III})}(\mathbf{k}) = \alpha k_+ e^{\frac{4}{3}\pi i} g(\mathbf{k}) - \bar{\alpha} k_- e^{-\frac{4}{3}\pi i} \bar{g}(\mathbf{k})$ is an analytic function of k_{\pm} and k_z satisfying $g(0, 0, k_z^{(0)}) = 1$, $g(\mathbf{k}) = g(C_6 \mathbf{k})$, and α is a complex constant. As well as the C_4 -symmetric case, the condition for nodal lines is decomposed into three cases, and $a_x^{(i)}(\mathbf{k}) = 0$ ($i = \text{I}, \text{II}, \text{III}$) represent three C_2 -symmetric surfaces, which are C_6 -symmetric in total. Therefore the evolutions of nodal lines occur on three surfaces containing the C_6 axis, and the events such as reconnection, annihilation, and creation are confined to each surface, and they follow C_6 symmetry in total. The topology change can be illustrated easily. It is similar to Fig. 9, only with the change from C_4 to C_6 , and so is omitted here.

- [1] X.-L. Qi and S.-C. Zhang, *Rev. Mod. Phys.* **83**, 1057 (2011).
- [2] M. Z. Hasan and C. L. Kane, *Rev. Mod. Phys.* **82**, 3045 (2010).
- [3] L. Fu and C. L. Kane, *Phys. Rev. B* **76**, 045302 (2007).
- [4] C. L. Kane and E. J. Mele, *Phys. Rev. Lett.* **95**, 146802 (2005).
- [5] C. L. Kane and E. J. Mele, *Phys. Rev. Lett.* **95**, 226801 (2005).
- [6] L. Fu, C. L. Kane, and E. J. Mele, *Phys. Rev. Lett.* **98**, 106803 (2007).
- [7] B. A. Bernevig, T. L. Hughes, and S.-C. Zhang, *Science* **314**, 1757 (2006).
- [8] N. P. Armitage, E. J. Mele, and A. Vishwanath, *Rev. Mod. Phys.* **90**, 015001 (2018).
- [9] C. Fang, H. Weng, X. Dai, and Z. Fang, *Chin. Phys. B* **25**, 117106 (2016).
- [10] H. Gao, J. W. Venderbos, Y. Kim, and A. M. Rappe, *Annu. Rev. Mater. Res.* **49**, 153 (2019).
- [11] B. Q. Lv, T. Qian, and H. Ding, *Rev. Mod. Phys.* **93**, 025002 (2021).
- [12] Z. Wang, Y. Sun, X.-Q. Chen, C. Franchini, G. Xu, H. Weng, X. Dai, and Z. Fang, *Phys. Rev. B* **85**, 195320 (2012).
- [13] S. M. Young, S. Zaheer, J. C. Y. Teo, C. L. Kane, E. J. Mele, and A. M. Rappe, *Phys. Rev. Lett.* **108**, 140405 (2012).
- [14] B.-J. Yang and N. Nagaosa, *Nat. Commun.* **5**, 4898 (2014).
- [15] X. Wan, A. M. Turner, A. Vishwanath, and S. Y. Savrasov, *Phys. Rev. B* **83**, 205101 (2011).
- [16] J. L. Mañes, *Phys. Rev. B* **85**, 155118 (2012).
- [17] A. A. Burkov and L. Balents, *Phys. Rev. Lett.* **107**, 127205 (2011).
- [18] B. Bradlyn, J. Cano, Z. Wang, M. G. Vergniory, C. Felser, R. J. Cava, and B. A. Bernevig, *Science* **353**, aaf5037 (2016).
- [19] C. Fang, L. Lu, J. Liu, and L. Fu, *Nat. Phys.* **12**, 936 (2016).
- [20] G. Chang, S.-Y. Xu, B. J. Wieder, D. S. Sanchez, S.-M. Huang, I. Belopolski, T.-R. Chang, S. Zhang, A. Bansil, H. Lin, and M. Z. Hasan, *Phys. Rev. Lett.* **119**, 206401 (2017).
- [21] S. Murakami, *New J. Phys.* **9**, 356 (2007).
- [22] A. A. Soluyanov, D. Gresch, Z. Wang, Q. Wu, M. Troyer, X. Dai, and B. A. Bernevig, *Nature (London)* **527**, 495 (2015).
- [23] H. Weng, C. Fang, Z. Fang, B. A. Bernevig, and X. Dai, *Phys. Rev. X* **5**, 011029 (2015).
- [24] B. Q. Lv, H. M. Weng, B. B. Fu, X. P. Wang, H. Miao, J. Ma, P. Richard, X. C. Huang, L. X. Zhao, G. F. Chen, Z. Fang, X. Dai, T. Qian, and H. Ding, *Phys. Rev. X* **5**, 031013 (2015).
- [25] S.-M. Huang, S.-Y. Xu, I. Belopolski, C.-C. Lee, G. Chang, T.-R. Chang, B. Wang, N. Alidoust, G. Bian, M. Neupane, D. Sanchez, H. Zheng, H.-T. Jeng, A. Bansil, T. Neupert, H. Lin, and M. Z. Hasan, *Proc. Natl. Acad. Sci. USA* **113**, 1180 (2016).
- [26] G. Chang, B. J. Wieder, F. Schindler, D. S. Sanchez, I. Belopolski, S.-M. Huang, B. Singh, D. Wu, T.-R. Chang, T. Neupert, S.-Y. Xu, H. Lin, and M. Z. Hasan, *Nat. Mater.* **17**, 978 (2018).
- [27] H. Park, W. Gao, X. Zhang, and S. S. Oh, *Nanophotonics* **11**, 2779 (2022).
- [28] B.-B. Fu, C.-J. Yi, T.-T. Zhang, M. Caputo, J.-Z. Ma, X. Gao, B. Q. Lv, L.-Y. Kong, Y.-B. Huang, P. Richard, M. Shi, V. N. Strocov, C. Fang, H.-M. Weng, Y.-G. Shi, T. Qian, and H. Ding, *Sci. Adv.* **5**, eaau6459 (2019).
- [29] M. Xiao, L. Ye, C. Qiu, H. He, Z. Liu, and S. Fan, *Sci. Adv.* **6**, eaav2360 (2020).
- [30] W. Wu, Y. Liu, S. Li, C. Zhong, Z.-M. Yu, X.-L. Sheng, Y. X. Zhao, and S. A. Yang, *Phys. Rev. B* **97**, 115125 (2018).
- [31] T. Bzdušek and M. Sigrist, *Phys. Rev. B* **96**, 155105 (2017).
- [32] Q.-F. Liang, J. Zhou, R. Yu, Z. Wang, and H. Weng, *Phys. Rev. B* **93**, 085427 (2016).
- [33] M. R. Khan, K. Bu, J.-T. Wang, and C. Chen, *Phys. Rev. B* **105**, 245152 (2022).
- [34] Y. Yang, J.-P. Xia, H.-X. Sun, Y. Ge, D. Jia, S.-Q. Yuan, S. A. Yang, Y. Chong, and B. Zhang, *Nat. Commun.* **10**, 5185 (2019).
- [35] C. Fang, Y. Chen, H.-Y. Kee, and L. Fu, *Phys. Rev. B* **92**, 081201(R) (2015).
- [36] A. A. Burkov, M. D. Hook, and L. Balents, *Phys. Rev. B* **84**, 235126 (2011).
- [37] Y.-H. Chan, C.-K. Chiu, M. Y. Chou, and A. P. Schnyder, *Phys. Rev. B* **93**, 205132 (2016).
- [38] L. M. Schoop, M. N. Ali, C. Straßer, A. Topp, A. Varykhalov, D. Marchenko, V. Duppel, S. S. P. Parkin, B. V. Lotsch, and C. R. Ast, *Nat. Commun.* **7**, 11696 (2016).
- [39] Y. Chen, Y.-M. Lu, and H.-Y. Kee, *Nat. Commun.* **6**, 6593 (2015).
- [40] Y. Kim, B. J. Wieder, C. L. Kane, and A. M. Rappe, *Phys. Rev. Lett.* **115**, 036806 (2015).
- [41] K. Mullen, B. Uchoa, and D. T. Glatzhofer, *Phys. Rev. Lett.* **115**, 026403 (2015).
- [42] T. Bzdušek, Q. Wu, A. Rüegg, M. Sigrist, and A. A. Soluyanov, *Nature (London)* **538**, 75 (2016).
- [43] R. Yu, Q. Wu, Z. Fang, and H. Weng, *Phys. Rev. Lett.* **119**, 036401 (2017).
- [44] Q. Yan, R. Liu, Z. Yan, B. Liu, H. Chen, Z. Wang, and L. Lu, *Nat. Phys.* **14**, 461 (2018).
- [45] W. Chen, H.-Z. Lu, and J.-M. Hou, *Phys. Rev. B* **96**, 041102(R) (2017).
- [46] Z. Yan, R. Bi, H. Shen, L. Lu, S.-C. Zhang, and Z. Wang, *Phys. Rev. B* **96**, 041103(R) (2017).
- [47] Y. Zhou, F. Xiong, X. Wan, and J. An, *Phys. Rev. B* **97**, 155140 (2018).
- [48] H. Park, S. Wong, X. Zhang, and S. S. Oh, *ACS Photon.* **8**, 2746 (2021).
- [49] E. Yang, B. Yang, O. You, H.-C. Chan, P. Mao, Q. Guo, S. Ma, L. Xia, D. Fan, Y. Xiang, and S. Zhang, *Phys. Rev. Lett.* **125**, 033901 (2020).
- [50] M. Wang, S. Liu, Q. Ma, R.-Y. Zhang, D. Wang, Q. Guo, B. Yang, M. Ke, Z. Liu, and C. T. Chan, *Phys. Rev. Lett.* **128**, 246601 (2022).
- [51] M. V. Berry, *Proc. R. Soc. London A* **392**, 45 (1984).
- [52] D. Xiao, M.-C. Chang, and Q. Niu, *Rev. Mod. Phys.* **82**, 1959 (2010).
- [53] D. Vanderbilt, *Berry Phases in Electronic Structure Theory: Electric Polarization, Orbital Magnetization and Topological Insulators* (Cambridge University Press, Cambridge, 2018).
- [54] M. Audin and M. Damian, *Morse Theory and Floer Homology* (Springer, London, 2014).
- [55] L. Nicolaescu, *An Invitation to Morse Theory* (Springer, New York, 2011).
- [56] H. Kamiya, *J. Fac. Sci., Shinshu Univ* **6**, 85 (1972).
- [57] R. S. Mulliken, *Phys. Rev.* **43**, 279 (1933).

- [58] C. J. Bradley and A. P. Cracknell, *The Mathematical Theory of Symmetry in Solids: Representation Theory for Point Groups and Space Groups*, Oxford Classic Texts in the Physical Sciences (Oxford University Press, New York, 2010).
- [59] P. M. Lenggenhager, X. Liu, S. S. Tsirkin, T. Neupert, and T. Bzdušek, [Phys. Rev. B **103**, L121101 \(2021\)](#).
- [60] J. Ahn, D. Kim, Y. Kim, and B.-J. Yang, [Phys. Rev. Lett. **121**, 106403 \(2018\)](#).